Main results of permafrost monitoring in the French Alps through the PermaFrance network over the period 2010–2022

Florence Magnin, Ludovic Ravanel, Xavier Bodin, Philip Deline, Emmanuel Malet, Jean-michel Krysiecki, Philippe Schoeneich

Received: 19 July 2022 | Revised: 4 September 2023 | Accepted: 22 September 2023

DOI: 10.1002/ppp.2209

RESEARCH ARTICLE

WILEY

Main results of permafrost monitoring in the French Alps through the *PermaFrance* network over the period 2010–2022

Florence Magnin[1] | Ludovic Ravanel[1] | Xavier Bodin[1] | Philip Deline[1] | Emmanuel Malet[1] | Jean-Michel Krysiecki[2] | Philippe Schoeneich[3]

[1]EDYTEM, Université Savoie Mont-Blanc, CNRS, Chambéry, France

[2]SAGE/ADRGT, Gières, France

[3]PACTE, Institut d'Urbanisme et de Géographie Alpine, Université Grenoble Alpes, Grenoble, France

Correspondence
Florence Magnin, EDYTEM, Université Savoie Mont-Blanc, CNRS, Chambéry, France.
Email: florence.magnin@univ-smb.fr

Funding information
Observatoire des Sciences de l'Univers de Grenoble; Observatoire des Sciences de l'Univers de Grenoble; EU POIA PermaRisk; EU Alpine Space PermaNET; EU Alcotra PrévRisk Haute Montagne

Abstract

This study presents data from the first years of permafrost monitoring in boreholes in the French Alps that started at the end of 2009 in the framework of the *PermaFrance* network. Nine boreholes are instrumented, among which six monitored permafrost temperature and active layer thickness (ALT) over >10 years. Ice-poor and cold permafrost in high-elevation north-facing rock walls has warmed by up to >1°C at 10 m depth over the reference decade (2011–2020), whereas ice-rich permafrost (rock glacier) temperatures remained stable. ALT has increased at four of the five boreholes for which decadal data are available. Summer 2015 marks a turning point in ALT regime and greatest ALT values were observed in 2022 (available for six boreholes), but thawing intensity did not show an obvious change. At one site with a layer of coarse blocks about 2 m thick, ALT was stable over 2018–2022 and response to the hottest years was dampened. Linear trends suggest an ALT increase of 2 m per decade for some ice-poor rock walls, independently of their thermal state. The data reveal a variety of permafrost patterns and evolution with significant intraregional and local differences. Snow modulates the response to air temperature signal in various ways, with an important effect on near-surface temperature trends and ALT: early snow melting in spring favors an ALT increase in rock walls. Maintaining these monitoring systems and understanding the physical processes controlling heterogeneous responses to climate signals is crucial to better assess permafrost dynamics and to adapt to its consequences.

KEYWORDS
active layer thickness, climate change, French Alps, monitoring, mountain permafrost, permafrost temperature

1 | INTRODUCTION

Permafrost is recognised as an essential climate variable (ECV) by the World Meteorological Organization.[1] Monitoring of permafrost temperature and active layer thickness (ALT, i.e., the depth of seasonal thaw) over long periods of time provides relevant information for understanding the impact of climate change on the cryospheric systems, the potential climate feedbacks through greenhouse gas release (e.g., Vonk and Gustafsson[2]), the implications for natural hazards driven by geomorphological processes (e.g., Hjort et al.[3]), and for cold

landscape evolution (e.g., Berthling and Etzelmüller[4]). Quantitative understanding of permafrost warming and degradation has become increasingly important in recent decades because of the risks to infrastructure and societies associated with landscape instabilities such as coastal retreat (e.g., Lantuit et al.[5]), thermokarst and thaw slumps (e.g., Lewkowicz and Way[6] and Luo et al.[7]), slope failures (e.g., Allen et al.[8] and Deline et al.[9]), and related cascading processes (e.g., Haeberli et al.[10]) and infrastructure damages (e.g., Hjort et al.[11]).

In the European Alps, the impacts of permafrost degradation have been documented, such as the increase in rockfall frequency[12,13] and high-magnitude rock avalanches,[14,15] the acceleration of rock glaciers and their potential destabilization,[16–19] sudden drainage of thermokarst lakes,[20] and destabilization of infrastructure.[21–23] As a result of these impacts, an adaptation strategy is also needed for mountain recreational practices, including mountaineering.[24,25]

Various regional and international permafrost monitoring projects have been established around the world and are relayed by the Global Terrestrial Network for Permafrost (GTN-P).[26] Most of the monitoring systems have been in place since the 21st century, so the existing time series are still relatively short. Nonetheless, assessments of the rate of permafrost change have been frequently reported for specific regions[27–32] and show that permafrost degradation is highly variable across and within regions.

On average, permafrost temperature increased by 0.39 ± 0.15°C at the global scale for continuous permafrost between 2007 and 2016,[33] which is similar to the average value reported for the European Alps over the last 20 years (0.4°C[29]). However, as a general pattern, ice-poor bedrock registered a much higher rate of warming (up to three times more than the average values[28,29]). The highly variable trends recorded within regions underline the need to extend the global monitoring system to remote regions and to better understand the effect of local conditions (snow, vegetation, ice content) on permafrost evolution.[34]

Schoeneich et al.[35] and Bodin et al.[20] summarized the first permafrost observations in the French Alps collected as part of the *Permafrance* network. The present study provides observations on geomorphological dynamics and ground temperature data to depths of 100 m obtained from six boreholes since late 2009. Since then, three more boreholes have been drilled and instrumented between 2017 and 2020. The objective of this paper is to describe the observations on permafrost patterns and dynamics from ground temperature monitoring during 2010–2022 in the French Alps, and discuss the effects of local conditions and the resulting intraregional variability of permafrost response to the climate signal.

2 | THE FRENCH ALPS

2.1 | General settings

The French Alps lie between the —N–s-oriented Rhône Valley, the Swiss and Italian borders, and the Mediterranean Sea, and cover ~50,000 km^2 over an area 250 km long and 50–75 km wide, distributed between 44 and 46°N and 5.7 and 7.7°E (Figure 1). They constitute the western part (~20%) of the European Alps and include 23 massifs that can be delineated based on topoclimatic parameters[38] and the summit of Mont Blanc at 4,809 m a.s.l.

Different meteorological dynamics shape the temperate climate of this chain, which is influenced both by the western flows of the Atlantic Ocean and by the southern flows of the Mediterranean Sea. A distinction is thus generally made between the Northern and Southern Alps, whose main break point is at ~45°N. The Northern Alps are generally higher, cooler, more humid, and more wooded and urbanized. They include the calcareous sub-alpine massifs (e.g., Vercors), the long depression of the *Sillon alpin*, the crystalline massifs, and the mainly crystalline central massifs, which extend from Mont Blanc to the Écrins, through Beaufortin, Belledonne, Vanoise, and Oisans. The southern French Alps are made up of sub-alpine massifs, the granitic massif of Mercantour, and the sedimentary nappes of the Briançonnais, Queyras, and Embrunais.

A latitudinal gradient of air temperature is recorded along the range, with a difference in mean annual air temperature of about 1.7°C at 1,800 m a.s.l. between the northernmost and the southernmost massifs, slightly greater in winter (1.8°C) than in summer (1.6°C[38]). The 0°C isotherm is thus located between 2200 m in the north and 2,700 m a.s.l. in the south. A longitudinal gradient of precipitation is observed: the northwestern side of the range, directly exposed to Atlantic influence, is wetter than the southeastern side, with differences of up to 1,148 mm per year, slightly higher in winter (628 mm) than in summer (543 mm). Topographic shelter effects locally affect this precipitation pattern. In the sheltered valleys and interior massifs such as Vanoise, Briançonnais, and Queyras, precipitation can be less than half that of the external massifs. About half of the precipitation at 1800 m altitude falls as snow in the northwest, while one-third falls as snow in the south. Due to the precipitation pattern and variability of the snow fraction, a gradient of snow accumulation is observed from northwest to southeast. However, snow accumulation has decreased below 2,700 m a.s.l. in the Northern Alps since the 1950s, whereas the trend is more regular in the Southern Alps.[39]

With an area of 275 km^2 in 2006–2009, the 548 glaciers covered less than 1% of the French Alps.[37] They were located in the Mont Blanc Massif (102 km^2 on the French side, 30.4 km^2 for Mer de Glace alone), Vanoise (93 km^2), and Écrins massifs (69 km^2). These massifs accounted for 96% of the glacierized area and 89% of the number of glaciers; the average glacier size was 0.5 km^2 while glaciers <0.5 km^2 accounted for 80% of all glaciers.[37] According to Paul et al.,[40] the total glacier area in the French Alps was 227 km^2 in 2015, with an overall decrease of 17% in 6–9 years due to current strong negative mass balances.[41]

2.2 | Permafrost extent

Typical mountain permafrost landforms are found in the French Alps and follow a north–south gradient similar to that of the climate parameters. The extent of permafrost in the French Alps has been

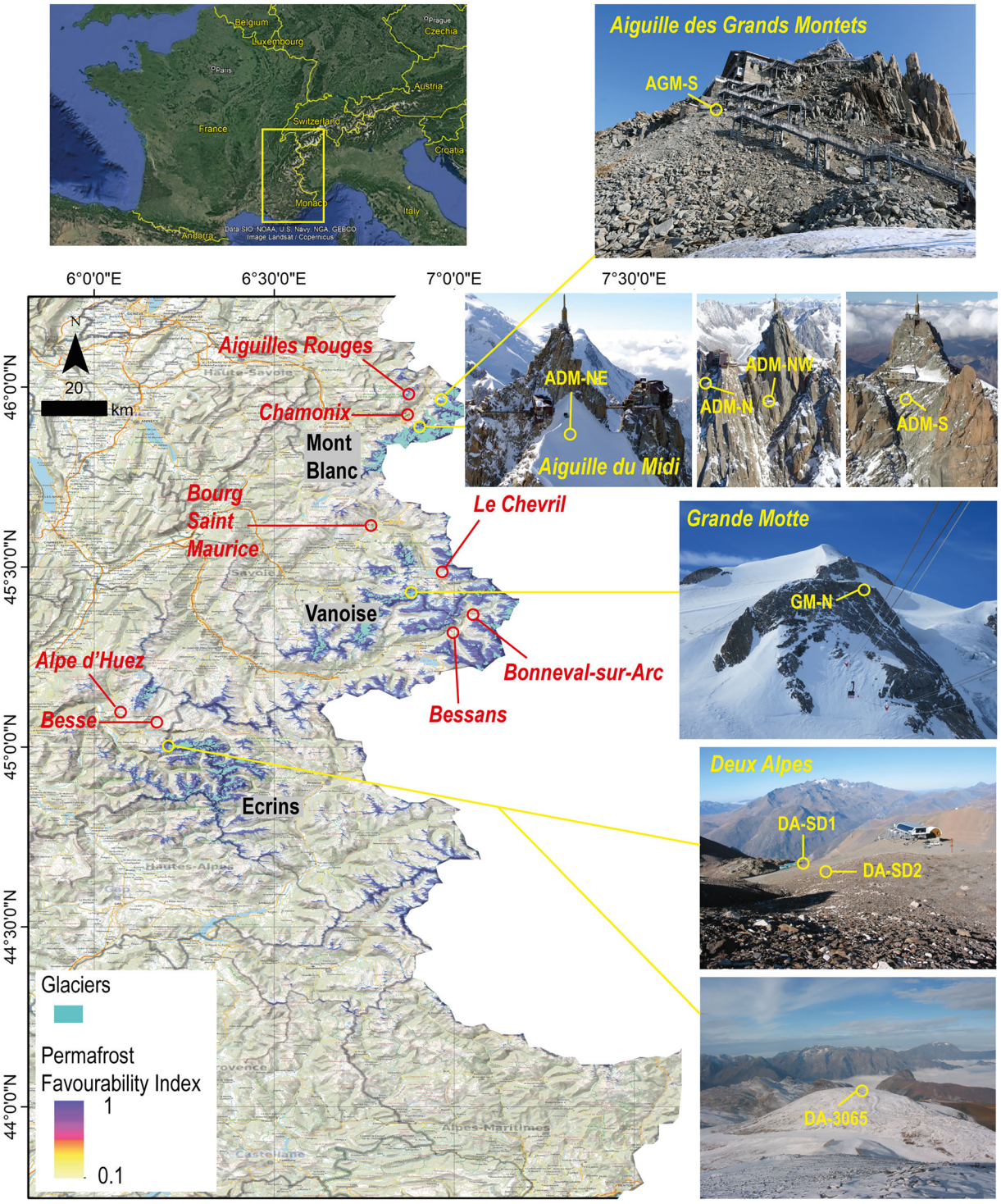

FIGURE 1 The French Alps with distribution of permafrost[36] and glaciers,[37] borehole sites (yellow), and weather stations (red). Additional images of the sites with more detailed views of the borehole locations are given in Figure S1. [Colour figure can be viewed at wileyonlinelibrary.com]

estimated using statistical modeling[36,42] to be between 700 and 1,500 km^2, that is, 10–20% of the areas above 2,000 m a.s.l.

Marcer et al.[36] showed that the lower limit of permafrost in areas of debris accumulation lies between 2,300 (north faces) and 2,700 m a.s.l. (south faces) in the northwestern French Alps, and 2,500 and 2,900 m a.s.l. in the southeastern areas. Since the 1990s, rock glaciers have accelerated and some have been destabilized.[19] Those located between 2,700 and 2,900 m on northern slopes are most susceptible to destabilization.[17] Two cases related to sudden rock glacier destabilization have been reported in the last two decades, including one that caused severe damage to ski and tourism infrastructure in Lanslevillard.[16,18]

Rock wall permafrost has been studied primarily in the Mont Blanc Massif. Magnin et al.[43] mapped the lower limit of discontinuous

permafrost at 2500 ± 200 m elevation in north faces and 3,000 ± 300 m in south faces for the period 1961–1990. Since the 1990s, the lower permafrost boundary has increased to at least 3,300 m in south-exposed rock faces,[44] and is mostly found at higher elevations, at least to 3,850 m, where snow accumulates in these sun-facing rock walls.[45]

Since the extremely hot summer of 2003, permafrost-affected rock walls in the French Alps have been increasingly affected by rockfalls and recent studies in the Mont Blanc Massif showed that they were related to hot summers[12] and extremely high temperature at the surface and depth of the scars.[46]

3 | PERMAFROST MONITORING SITES IN THE FRENCH ALPS

The French monitoring network of mountain permafrost, called *PermaFrance*, was set up in 2009[35] with support of the OSUG (*Observatoire des Sciences de l'Univers de Grenoble*). It is devoted to the monitoring of permafrost temperature, ALT, and related geomorphological processes (rock falls and rock glacier velocity) in the French Alps. It contributes data to the GTN-P and is part of the French OZCAR research infrastructure on the Critical Zone. We present and comment here only the data from the borehole sites.

3.1 | The Aiguille du Midi: four boreholes

The Aiguille du Midi (ADM, 3,842 m a.s.l.) is the highest and most western summit of the Aiguilles de Chamonix, located on the NW flank of the Mont Blanc Massif. It is located in the inclusion-rich porphyritic granite area of the massif and is bounded on its north and west sides by the wide Angle Fault at the contact between granite and gneiss. It includes three peaks that are all connected by bridges and galleries: the Piton Nord which stands ~1,000 m above the Pélerins and Bossons Glaciers and hosts the upper station of the ADM cable-car to Chamonix, Piton Central which is the highest peak and hosts the station of the *Panoramic Mont-Blanc* to Pointe Helbronner, and finally, Piton Sud which stands ~250 m above the Géant Glacier.

Three 66-mm-diameter boreholes were drilled up to 11 m depth, perpendicular to the rock surface at Piton Central in September 2009: ADM-S on the lower part of the SE face, which is the most gently inclined, and ADM-NE and ADM-NW on the NE and NW faces respectively (Figure 1, Table 1). Details of the borehole settings are also provided in Magnin et al.[47] In 2020, a fourth 11-m-deep borehole (ADM-N) was drilled on the north face of Piton Nord.

The boreholes were equipped with thermistor strings calibrated in an ice-water bath and then inserted into 32-mm high-density polyethylene pipe. In September 2017, thermistor strings were replaced at ADM-S and ADM-NE after several sensor failures. Instrumentation details are provided in Table 2 and data availability is displayed in Figures 2 and S2.

3.2 | Les Deux Alpes: three boreholes

The Deux Alpes (DA) ski resort is located in the northwestern part of the Écrins massif and is mainly developed on the exhumed ante-Triassic erosion surface which crosses the gneiss basement. Three vertical boreholes were drilled on two sites of the ski resort.

Two 15-m-deep boreholes (DA-SD1 and DA-SD2) were drilled in 2009 on the Bellecombe rock glacier (2,700–2,750 m a.s.l.) near a chairlift station. The rock glacier, made of limestone blocks flowing on a gneiss base, presents discrete landforms; GNSS measurements indicate a low velocity, in the decimeter range. The two boreholes are ~50 m apart and have similar profiles. The temperature is measured every 6 h to a depth of 4.5 m, and every 12 h at greater depth.

At DA-SD1, the loggers were damaged by water in 2017 and had to be replaced in 2018. Its concrete casing was also damaged by ski-run engines during winter 2020/21; subsequently, the borehole string was removed in summer 2021.

A 100-m-deep borehole (DA-3065) was drilled in 2010 at 3065 m elevation on an undisturbed area at the edge of the ski resort, in accordance with PACE project standards.[30] The borehole was drilled over a large, homogeneous gneissic dome to characterize the long-term evolution of the thermal profile of the bedrock. Temperature is measured every 6 h down to 11 m, and every 12 h further down.

A distributed temperature sensing (DTS) fiber optic cable was also added in the borehole for additional measurements and verification of the temperature sensors. The 700-m-long optic fiber cable was installed in two loops: one taped on the outside of the casing tube, and another pushed down into the tube along with the sensor chain. This setting allows four parallel profiles to be measured at each measurement run. The fiber can be measured in both directions, giving up to eight profiles that can be averaged to reduce noise. The DTS was measured episodically. Each measurement session needs to be calibrated in an ice-water bath. Details on the setting, the protocol, and the data processing are given in Schoeneich et al.[48,49] and Table 2.

The borehole has experienced numerous problems since installation[50] including logger and sensor failures that there are limited data available after 2012.

3.3 | Aiguilles des Grands Montets: one borehole

On the NE side of the Mont Blanc Massif, the Aiguilles des Grands Montets (AGM, 3,296 m a.s.l.) is the highest summit of the Lognan – Les Grands Montets ski area (Chamonix) and was accessible by cable-car until 2019 when a fire destroyed the departure station. It is a pyramid-shaped peak with a triangular base around which four glaciers flow: Rognon Glacier to the east, Lognan and Pendant Glaciers to the NW, and the remains of Grands Montets Glacier to the SW. The bedrock is granite but its proximity to the Angle Fault explains its very unstructured character on the moderately steep (45–55°) NW and SW slopes. The steeper east face is also very fractured. Slopes have modest height, with a maximum of 250 m on the NW one. The SW slope, on which the borehole is located, is the gentlest

TABLE 1 Borehole topographical and morphological characteristics.

ID	Massif	Ground type (surface)	Elevation (m a.s.l.)	Aspect (°)	Slope (°)	Borehole depth and inclination	Comments
ADM-S	Mont Blanc (MBM)	Bedrock	3,753	185[a]	55	10 m Normal to slope	Fractured and rugged bedrock, snow accumulation that can locally reach >1 m
ADM-NE			3,738	75[a]	65	10 m Normal to slope	Fractured rock with heterogeneous snow deposits generally <0.5 m
ADM-NW			3,745	270[a]	90	10 m Normal to slope	Homogeneous bedrock at the surface, borehole crosses an open fracture at ~2.5 m depth and is located right above a ledge where thick snow (1 m) accumulates and cover the borehole entrance
ADM-N			3,754	345	77	10 m Normal to slope	Homogeneous and very little fractured bedrock over the entire borehole
AGM-S		Bedrock	3,242	183	42	17 m Normal to slope	Coarse blocks in the shallowest meters, bedrock at depth, snow-covered site
DA-SD1	Ecrins	Rock glacier	2,710	340	10	15 m Vertical	Unfrozen coarse debris down to 1.7 m, unfrozen debris with fine matrix down to 2.3 m, ice-rich debris down to 4.8 m, ice with stones down to 9.7 m, bedrock below, snow-covered site
DA-SD2			2,725	340	5	15 m Vertical	Debris down to 2.2 m, ice-rich debris down to 9.5 m, bedrock below, snow-covered site
DA-3065		Bedrock	3,065	—	0	100 m vertical	Frost-shattered bedrock up to 2 m thick, and moderately fractured bedrock deeper. Windblown location. Shallow snow accumulation
GM-N	Vanoise	Bedrock	3,355	345	58	20 m Normal to slope	Fractured bedrock, mostly snow free

Note: The borehole IDs are the same as those in the GTN-P database.
[a]These values are corrected compared to those in Magnin et al.,[47] in which inaccurate values were reported: 135° for ADM-S (BH_S), 50° for ADM-NE (BH-E), and 345° for ADM-NW (BH_N).

and smallest (about 80 m). The 17-m-deep borehole (AGM-S), was drilled perpendicular to the slope in 2016, is located in a south-facing area of disjointed blocks. The borehole was equipped with a thermistor string inserted into a 76-mm PVC tube. Data are collected every 3 h.

3.4 | Tignes – La Grande Motte: one borehole

La Grande Motte (GM, 3653 m a.s.l.) is a summit of the Vanoise Massif dominating the ski area of Tignes. Its south face is unglaciated while the Grande Motte glacier flows on the north side. From the summit, a rock ridge that was still largely ice-covered three decades ago now divides the glacier into two parts along a length of 1.3 km. At mid-distance on this ridge, a main 200-m-high spur is present on the top of which the only pylon of the Grande Motte cable-car (reaching 3,456 m a.s.l.) has been built on a flat area at 3,375 m a.s.l. The borehole (GM-N), drilled in 2019, is 20 m deep, perpendicular to the surface of the north-facing rock (Malm limestone). It is located about 20 m downstream (at 3,355 m a.s.l.) from the pylon. The instrumentation and data collection setting are identical to AGM-S.

4 | DATA AND PROCESSING

4.1 | Climate data

Air temperature and precipitation trends over the past four decades were calculated to describe the climate settings of the Mont Blanc, Vanoise, and Écrins massifs. The closest meteorological stations of each monitoring site with the most continuous data since at least 1981 were used (Figure 1): Chamonix (1,042 m a.s.l.) located 5 and 7.5 km northwest and southwest of ADM and AGM, respectively;

TABLE 2 Borehole instrumentation and installation.

ID	Starting date (dd.m.yr)	Temperature measurement system	Sensor depths (m)	Logger
ADM-S	18.12.2009	YSI 44031 Stump ForaTech AG thermistors (acc. ±0.1°C) replaced in September 2017 by YSI 55031	0.14, 0.34, 0.54, 0.74, 1.04, 1.34, 1.64, 2.14, 2.64, 3.64, 4.64, 6.64, 8.64, 9.64	Campbell CR1000
ADM-NE	13.04.2010		0.3, 0.5, 0.7, 0.9, 1.1, 1.4, 1.7, 2; 2.5, 3, 4, 5, 7, 9, 10	
ADM-NW	16.12.2009	YSI 44031 Stump ForaTech AG thermistors (acc. ±0.1°C)		
ADM-N	24.09.2020	YSI 55031 Geokon thermistors		Campbell CR1000X
AGM-S	09.09.2017	YSI 55031 Geokon thermistors	0.3, 0.6, 1, 1.5, 2, 3, 4, 5.5, 7, 8.5, 10, 11.5, 13, 15, 17	Campbell CR1000
DA-SD2	21.11.2009	TCSA PT100 sensors (acc. ±0.1°C) ($n = 15$)	0.2, 0.6, 1.1, 1.6, 2.6, 3.6, 4.6, 5.6, 6.6, 7.6, 8.6, 10.1, 12.1, 13.6	Paratronic
DA-SD1	21.11.2009	TCSA PT100 sensors (acc. ±0.1°C) ($n = 15$)	0.2, 0.7, 1.2, 1.7, 2.7, 3.7, 4.7, 5.7, 6.7, 7.7, 8.7, 10.2, 12.2, 13.7	Paratronic and Campbell CR300 logger from 2018
DA-3065	14.12.2010	TCSA PT100 sensors (acc. ±0.1°C) ($n = 30$)	0.2, 0.6, 1, 1.5, 2, 2.5, 3, 4, 6, 8, 10, 12, 14, 16, 19, 24, 29, 34, 39, 44, 49, 59, 69, 79, 89, 94, 99	Paratronic and Campbell CR1000 since 2014
		Optical fiber (DTS) (50/125 µm quartz graded index multimode fiber optic cable) (total length 700 m, 400 m in borehole)	DTS resolution 1 m until 2014, 0.5 m after 2014 Four duplicate profiles	APSensing Agilent (2011 to 2014) and Silixa in 2014
GM-N	19.11.2020	YSI 55031 Geokon thermistors	0.3, 1, 1.5, 2, 2.5, 3, 4, 5, 6.5, 8, 10, 12, 14.5, 17, 20	Campbell CR1000

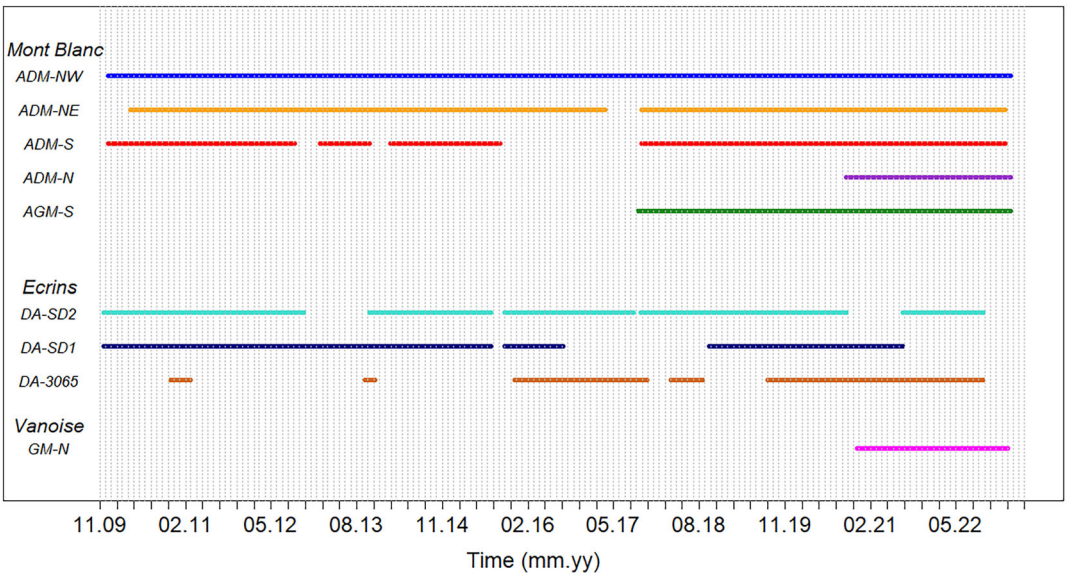

FIGURE 2 Borehole data availability. Horizontal bars represent periods when data for all sensors of a single boreholes are available. DA-SD1 was closed in 2021 but for the other boreholes the bars stop when last data collections were performed. A more detailed figure displaying availability per sensor is reported in the supporting information (Fig. S2). [Colour figure can be viewed at wileyonlinelibrary.com]

Besse (1,520 m) located ~8 km north of the Deux Alpes sites; and Bourg Saint Maurice (865 m) and Bessans (1713 m) located ~24 km north and ~14 km southwest of La Grande Motte, respectively. For the last, we considered two stations because it is located in a zone of different influences, with an effect in terms of snow accumulation[39]: Bourg Saint Maurice is mainly exposed to Atlantic influence despite its sheltered position in the Alpine range, while Bessans is more exposed to the advection of humid Mediterranean air masses.

Daily means of air temperature were calculated from daily minimum and maximum values (TNTXM). Daily precipitation was first aggregated into an annual value. For each time series, the average of the normal period 1981–2010 was first calculated and then anomalies

to this period were calculated for each year between 1981 and 2022. For Bessans, air temperature has only been recorded since 1984; the anomalies in relation to the 1981–2010 normal were therefore not calculated for this station.

For Besse weather station, 4.6% of the TNTXM data are missing and were filled with linear regression using the nearby Alpe d'Huez weather station. The fitted linear regression between the TNTXM of the two stations for the available data during the period 1981–2010 shows an R^2 of .95.

We additionally aggregated the data into seasonal means: winter (DJF), spring (MAM), summer (JJA), and autumn (SON) for the borehole measurement period (2010–2022) to allow for an in-depth analysis of climatic conditions over the measurement period. Trends for each season and each station were calculated from the slope of a linear regression fitted between air temperature and time (seasons or days) over the decade 2011–2020 which we used as the reference decade to report permafrost changes and compare sites with each other.

Finally, to analyse the annual variability of each site, we also considered snow depth data collected at neighboring stations where snow parameters are monitored: Aiguilles Rouges (2,330 m a.s.l.) for the Mont Blanc Massif, Le Chevril (2,560 m) and Bonneval (2,720 m) for the Vanoise Massif, and Les Deux Alpes (2550 m) for the Écrins Massif. Here again, two weather stations were considered for the Vanoise Massif due to its position on a climatic divide between Atlantic and Mediterranean influences.

4.2 | Borehole data

4.2.1 | Borehole temperature data processing

The analysis considered ALT and permafrost temperature. We aggregated the raw ground temperature data into daily and annual means. Annual means were aggregated according to hydrological years (1 Oct. to 30 Sep.). We also analysed ground temperature data through 31-day and 365-day running means.

Six boreholes (ADM-NW, ADM-NE, ADM-S, DA-SD1, DA-SD2, and DA-3065) have recorded data for more than a decade and we used the reference decade 2011–2020 (hydrological years) to report on ground temperature evolution and to compare sites with each other as well as with other regions of the European Alps and the world, despite the limitations of the latter comparison due to slight mismatches in reference periods. Trends were calculated based on a linear regression between the time (days) and temperature smoothed with 365-day running means. When temperature records were affected by gaps due to sensor failure or logger removal, annual means were not computed but linear interpolation was applied to the 365-day running means to fill the gaps when calculating decadal trends. In one borehole (DA-SD1) temperature anomalies were sometimes recorded and it was difficult to assess whether these were associated with natural processes or caused by sensor drift. We therefore retained these data and provided an interpretation regarding processes causing these anomalies but avoided interpreting trends. Statistical significance of the decadal trend was analysed using *p*-values: when *p*-values are >.05, their significance is poor, and we mention this when presenting the trend. If we do not mention the *p*-values, this means that the statistical significance is high (<.05).

Near-surface sensors sometimes recorded zero curtain (ZC) periods when the ice-rich surface layer thawed together with snow melting[51]: surface temperature stagnated at or close to 0°C until complete melting. We calculated near-surface ZC from the shallowest sensors where relevant. A ZC effect was detected with temperature ranging between −0.2 and 0.2°C (considering temperature sensors with 0.1°C resolution) after winter freezing, and with day-to-day change ≤0.1°C.

4.2.2 | Determination of the ALT parameters

Maximum ALT was determined for each year using linear interpolation between the deepest sensor that recorded a positive temperature and the next sensor that did not record a positive temperature and using daily temperature data. Uncertainty in the results is thus related to the sensor spacing and is more pronounced in ice-rich permafrost such as for DA-SD1 and DA-SD2 where latent heat uptake plays a major role in the heat diffusivity until ground ice has melted.[52] Haberkorn et al.[29] further introduced the concept of mean annual ALT (MAALT), which depicts the duration and intensity of seasonal thaw. Following their approach, we completed our analysis with MAALT values that are the mean of the daily ALT for 1 year.

4.2.3 | Optic fiber data processing

The raw DTS measurements first had to be corrected for instrument offset and signal loss with distance. For this, three sections of fiber optic cable (first 100 m, a 100-m section between the outer and inner loops, last 100 m) were plunged into an ice-water bath for calibration. These sections at 0°C were then used for correction of both the offset and the trend. Once corrected and calibrated, the four downward and upward profiles could be extracted from the data. Upward profiles were inverted. A 30-cm section 1 m above the borehole top was wrapped in a black plastic bag to induce a warm peak in the record, which is used to align the four profiles. The parallel profiles could be averaged to reduce noise, and absolute differences and standard deviation were calculated to evaluate uncertainty. The results were compared with a reference sensor (29 m) to check accuracy. More details on data processing are given in Schoeneich et al.[49]

Every measurement run provided four parallel profiles. When several runs were performed (typically in both directions to minimize the effect of possible fiber cable defects), up to eight or more profiles could be averaged. In 2013, four seasonal measurement sessions were performed at 3-month intervals, allowing the determination of depth of the zero annual amplitude (ZAA) at ~25–30 m depth.

Since the DTS was measured episodically, it was used in parallel with the sensor chain: the DTS provided a complete and detailed

profile, while the sensors provided the temporal evolution. The DTS also allowed identification of deviation in sensors and elimination of unreliable sensors from analysis (see Section 5.6).

5 | RESULTS AND PRELIMINARY OBSERVATIONS

5.1 | Climate conditions

5.1.1 | Climate conditions over the past four decades

Mean air temperature during the period 1981–2010 was +7.33°C at Chamonix, +9.08°C at Bourg Saint Maurice, and +6.94°C at Besse. These values are 0.79, 0.96, and 0.96°C higher than the 1961–1990 average, respectively. Annual temperature anomalies compared to the 1981–2010 average are displayed in Figure 3(a) for the three stations.

Since 2011, annual mean temperature at all sites has exceeded the 1981–2010 average by more than 2°C in some years. The warmest year was 2022 at all stations. Since 1997, only 2010 has been below this average at Besse, and 2005 and 2010 for the other stations. During the decade 2011–2020, mean air temperature relative to the period 1981–2010 was +1.25°C at Chamonix, +1.5°C at Bourg Saint-Maurice, and +2.13°C at Besse, with linear trends ranging from +1.14 to +1.39°C within the decade (Figure 3c).

Precipitation trends were less clear, but all four stations were globally wetter during 1999–2003 and drier since 2003 compared to the 1981–2010 average (Figure 3b). Unlike air temperature, not all stations had similar anomalies from year to year: for example, the anomaly was negative at Chamonix but positive at the other stations in 2018. In recent years, Bessans has recorded the highest positive anomaly (>+300 mm in 2018) and Chamonix the lowest one (down to −200 mm in 2017). Bessans also showed opposite trends to the other stations for some years: for example, all stations recorded a negative anomaly in 2011, except Bessans, with the

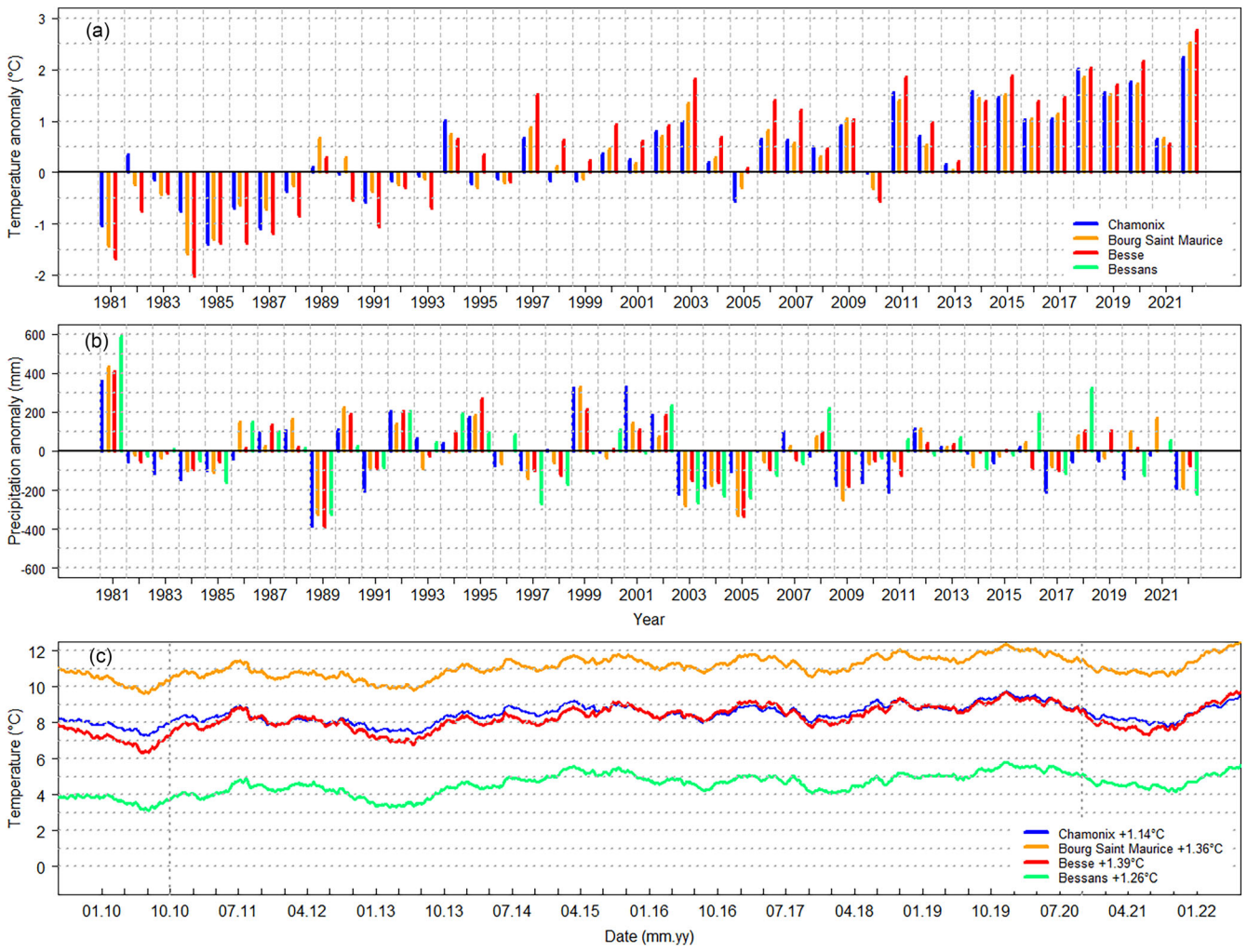

FIGURE 3 Air temperature (a) and precipitation (b) anomalies compared to the 1981–2010 average air temperature and precipitation; (c) daily air temperature data filtered with a 365-day running mean over the last decade, with linear trend values during the reference decade (vertical dotted lines delineate the decade). [Colour figure can be viewed at wileyonlinelibrary.com]

opposite in 2012. This specific trend at Bessans reveals the influence of moist air flows from the southeast, typical of areas near the main divide (see Section 3.1).

5.1.2 | Seasonal trend over the permafrost observation period

Over all years of borehole temperature measurement (2010–2022), the warmest winters (DJF) occurred in 2016 and 2020 for all stations (Figure 4a), the warmest springs (MAM) in 2011, 2020, and 2022 (as well as 2015 and 2017 at Bessans, Figure 4c), the warmest summers (JJA) in 2015, 2017, 2018, 2019, and 2022 (Figure 4e), and finally the warmest autumns (SON) in 2014, 2018, and 2022 (Figure 4g). Conversely, 2012 and 2013 had cold winters, 2013 and 2021 had cold springs, 2014 had a cold summer, and the coldest autumn was in 2017. In terms of precipitation, the winter of 2018 was wetter at all stations and in 2017 drier (as well as 2021 at Besse, Figure 4b). Snow thickness in 2018 was thus the highest for some stations (Aiguilles Rouges and Bessans) and relatively high for the other stations. Registered lowest snow thicknesses was in 2011, 2014, and 2015 (Figure 4i).

Despite their relative vicinity, Bourg Saint-Maurice and Bessans had respectively the wettest and driest winter conditions of all four stations, for the reasons exposed in Section 3.1. Chamonix was the wettest station for the other seasons, notably in summer (Figure 4d,f,h). As for the four-decades trend, Bessans recorded annual variations different from those of the other stations due to the Mediterranean influence, with, for example, a particularly rainy autumn in 2016 when it was average for the other stations. Summer 2014 was particularly wet at all stations and compared to 2018 which was particularly dry. However, other years with similarly warm or dry conditions were registered for some stations.

Linear trends (based on the slope of linear regressions) during the reference decade (2011–2020) show that winter was the season that experienced the greatest warming: from 2.64°C at Bourg Saint-Maurice to 3.65°C at Besse, and the greatest increase in precipitation, from 88.6 mm at Chamonix to 145 mm at Besse. Summers have also warmed significantly: from 1.7°C at Chamonix to 2.26°C at Bourg Saint Maurice, but precipitation has decreased during this season,

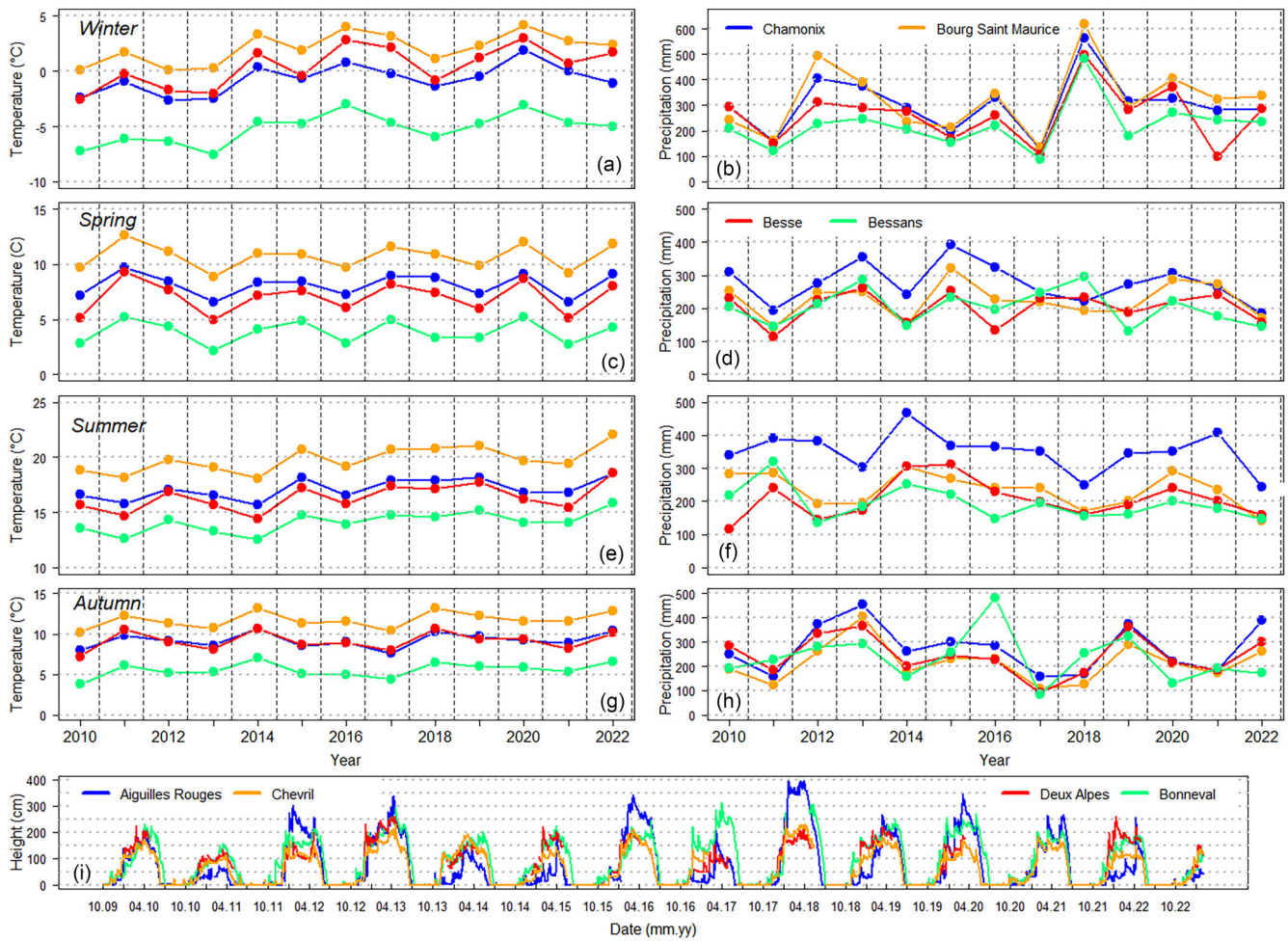

FIGURE 4 Seasonal air temperature (a, c, e, g) and precipitation (b, d, f, h), as well as daily maximum snow height at the different weather stations (i). [Colour figure can be viewed at wileyonlinelibrary.com]

from 8.2 mm at Besse to 78.9 mm at Bessans. A slight decrease in temperature was recorded in spring (from 0.04 to 0.2°C) and variable trends but close to 0°C trends were recorded in autumn (from −0.24°C at Besse to +0.29°C at Bourg Saint-Maurice). In terms of precipitation, spring and autumn had slightly contrasting trends, with a general increase in spring (from 15.3 to 43.8 mm) and a general decrease in autumn (from 37.4 to 72.7 mm). Nonetheless, none of these seasonal trends are statistically significant, with *p*-values ranging from .05 to 1.

5.2 | Near-surface temperature

Temperature evolution at the near-surface (that is here displayed with records at the shallowest sensor of each borehole which are typically <0.5 m depth) is displayed with 31- and 365-day running means and with calculated decadal trends from the slope of linear regression (see Section 4.2.1) in Figure 5. The highest temperature recorded in summer was found at DA-SD2, followed by AGM-S, ADM-NE, ADM-S, and DA-3065 (Figure 5a). No distinction between ice-rich and ice-poor sites or snow-free and snow-covered sites could be made for these highest values with a 31-day running mean. Lowest values recorded in winter were at the north-exposed and snow-free sites ADM-N, GM-N, and ADM-NE. The snow-covered ADM-NW surface had slightly higher temperature values in winter than the other north-facing boreholes.

The 365-day running means show two distinct groups of boreholes. (a) The relatively warm ADM-S, DA-3065, DA-SD1, DA-SD2, and AGM-S, with close to 0°C or positive temperature (Figure 5b) are on sun-exposed or flat and snow-covered ground. (b) The cold ADM-NE, ADM-NW, and GM-N (Figure 5c) are those receiving little solar radiation, are located at higher elevations, and are either snow-covered (ADM-NW: local and thick snow accumulation) or snow-free. Trends over the reference decade are available for five boreholes; there is a clear difference between warm and snow-covered permafrost and cold and snow-free permafrost: the decadal trend at ADM-S was 0.88°C lower than the air temperature trend at Chamonix, and 0.31°C higher at ADM-NE. The most contrasting surface temperature trends were thus found on the same site at Aiguille du Midi, which reveals the complex control of solar radiation and variable snow cover. At DA-SD1 and DA-SD2, the near-surface temperature trend was respectively 0.81 and 0.72°C lower than the air temperature increase at Besse.

Only DA-SD1, DA-SD2, and DA-3065 showed recurrent ZC with the 31-day running mean (Figure 5a). Figure 6(a) displays the duration

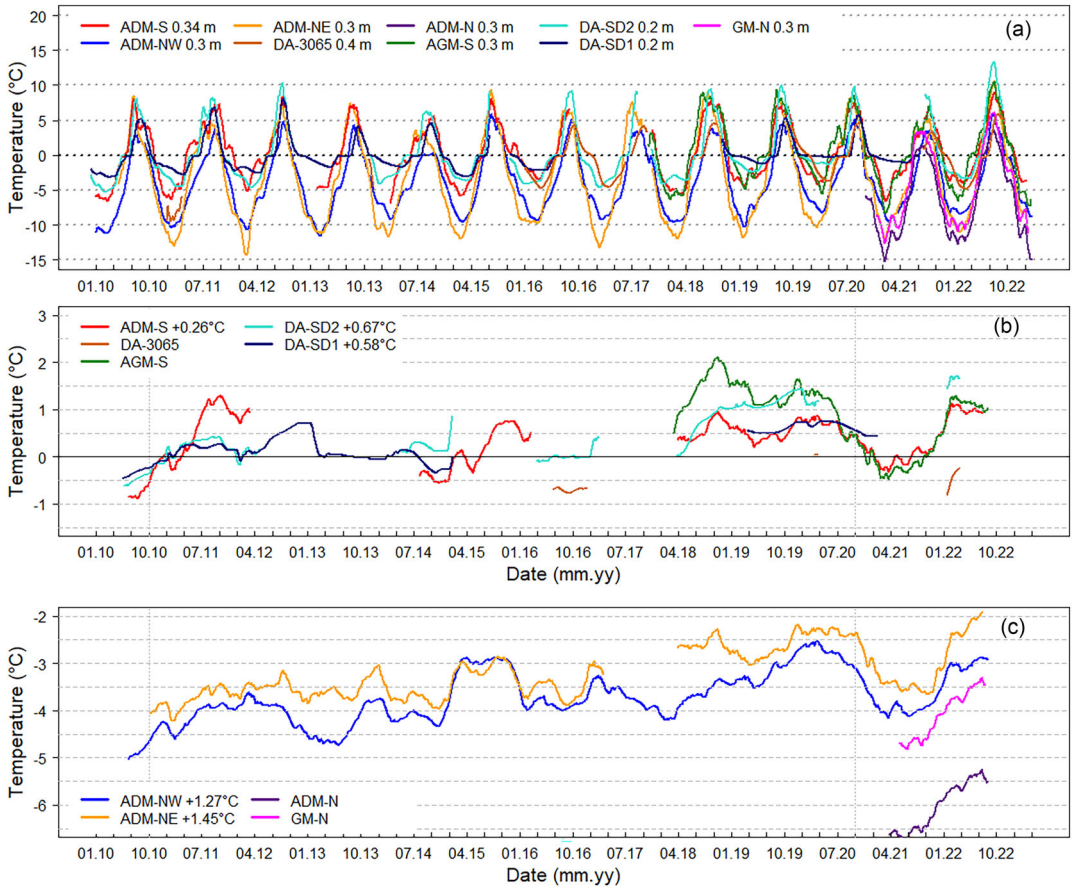

FIGURE 5 Near-surface temperature displayed with: (a) a 31-day running mean—depths of the near-surface sensors are given with the borehole names; (b, c): a 365-day running mean (linear trends over the reference decade are given in the keys, vertical dotted lines delineate the decade). [Colour figure can be viewed at wileyonlinelibrary.com]

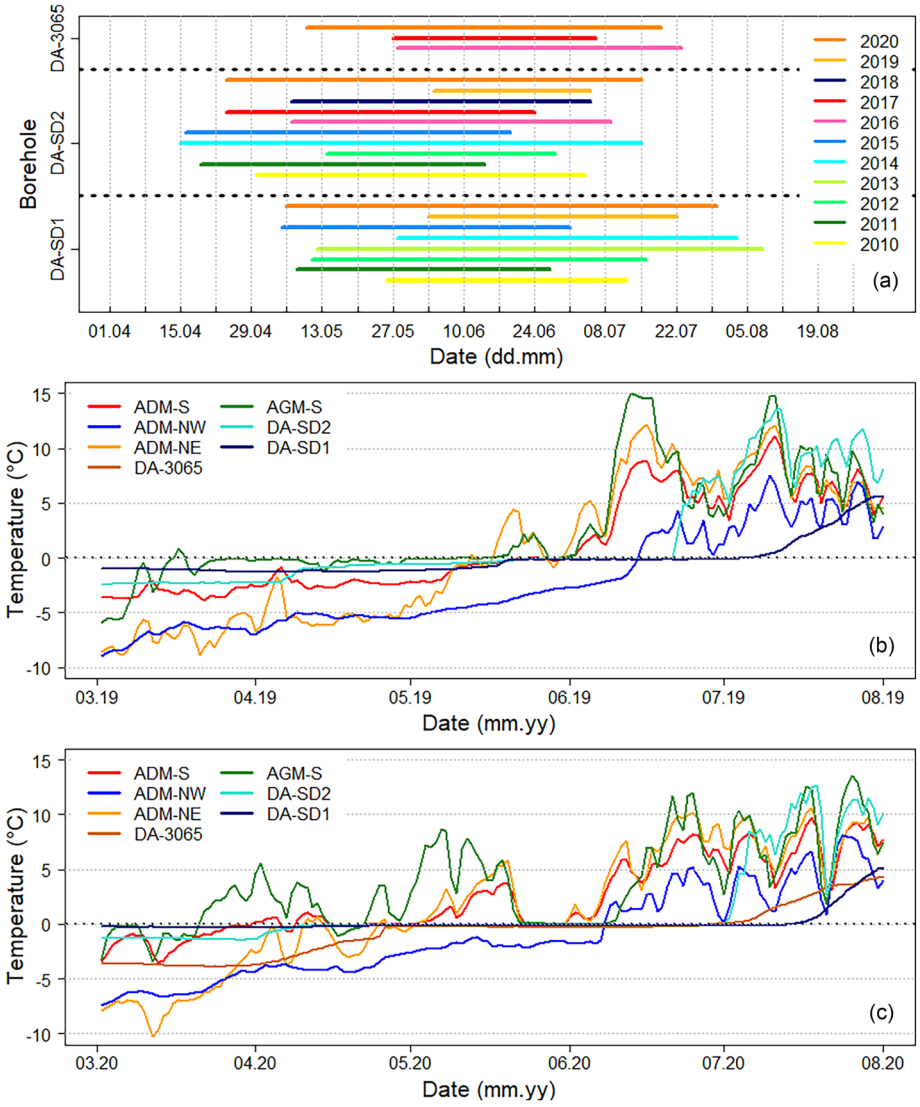

FIGURE 6 Dates and duration of near-surface zero curtain measured at 0.2 m depth (a), and example of daily temperature records during spring and summer 2019 (b) and 2020 (c) showing the dampening effect of snow at 0.2 (DA-SD1, DA-SD2, DA-3065), 0.3 (ADM-NW, ADM-NE), and 0.34 m (ADM-S). [Colour figure can be viewed at wileyonlinelibrary.com]

of near-surface ZC caused by snow melting at the gently inclined sites (the Deux Alpes boreholes). At the steep slope sites of ADM-NW, ADM-S, and AGM-S where snow also accumulates at the surface, ZC was not observed but a dampened daily temperature change could be observed in spring and early summer (Figure 6b,c). Periods of continuous temperature close to 0°C were sometimes observed at the surface (e.g., from mid-May to early June 2019 at AGM-S) but occurred after periods of positive surface temperature, showing effects of late snow falls after a drier period with snow removal in spring and was also marked by spells of lower temperature. ZC generally began (up to >1 month) and ended earlier (1–2 weeks) at DA-SD2 than at DA-SD1, and sometimes persisted well into the summer at DA-SD1 (e.g., 2013 and 2014). In 2011, which was a year with little snow accumulation (Figure 4i), ZC ended relatively early while in 2013, which registered the greatest snow thickness at the Deux Alpes, ZC lasted until early August at DA-SD1. At DA-3065, ZC started later and lasted shorter probably because of its wind-blown position causing a limited snow thickness (Table 1). Comparison of these sites illustrates the highly heterogeneous effect of snow on surface temperature within the same area.

5.3 | Active layer thickness

ALT varied significantly both spatially (from one borehole to another) and temporally (day of maximum recorded) as shown in Figures 7 and 8 and Table S1. ALT was thinner and more stable in ice-rich (especially DA-SD2) than in ice-poor materials where it showed high interannual but also reversible variations (Figures 7 and 8). However, no major difference in terms of changes was observed between bedrock permafrost and rock glaciers over the measurement period, with a maximum change of 48% between 2010 and 2020 (years selected to ensure comparisons between boreholes) at ADM-NE, 41% at ADM-NW, 36% at ADM-S, or 34% at DA-SD2.

Maximum ALT was reached as early as June at DA-SD2 in 2011, 2012, and 2014 (no data in 2013) but as late as mid-November at ADM-S in 2018 and 2019. At DA-SD2, maximum ALT occurred early in the summer and sometimes before total snow melt (Table S1) until 2014 because of melt water infiltration in the porous blocky surface layer. The top of this ice-rich permafrost was marked by an important ZC that started before or concomitantly with surface thaw and lasted well after surface refreeze (Figure 8).

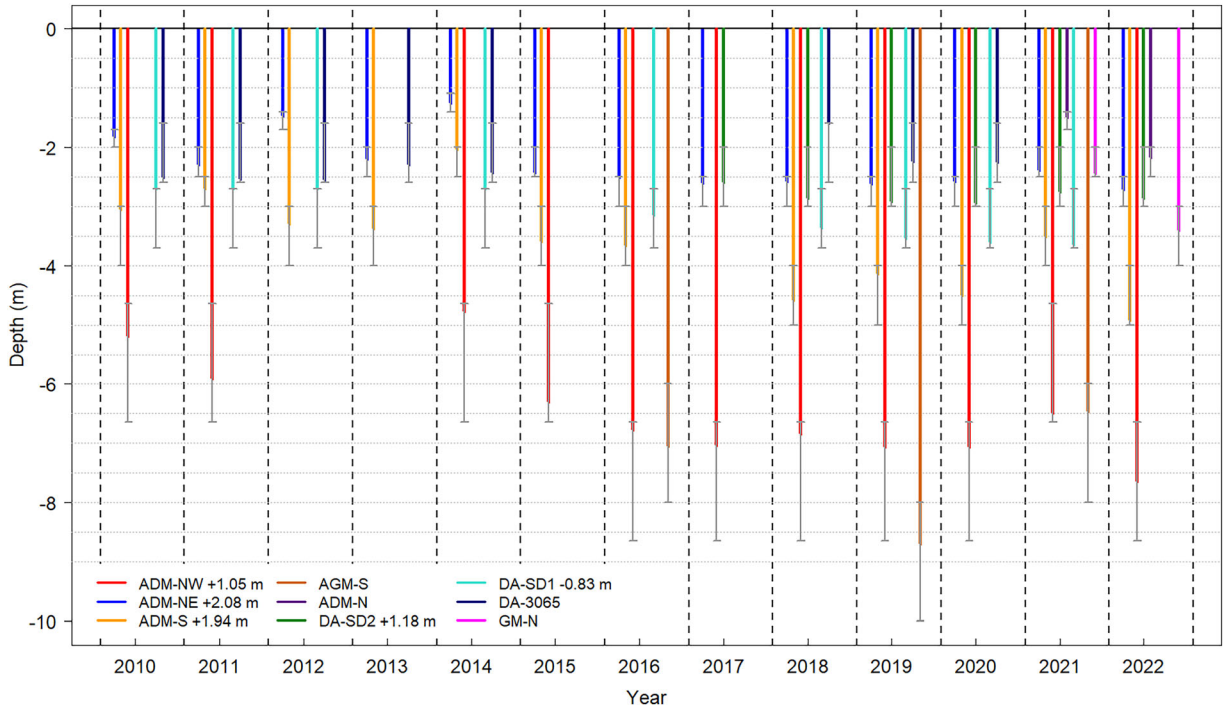

FIGURE 7 Maximum ALT recorded for each year of full record during the thawing season at each borehole. Error bars indicate sensor depths between which the ALT value was interpolated; linear trends over the reference decade (2011–2020) are given in the key where available. [Colour figure can be viewed at wileyonlinelibrary.com]

Since 2015, ALT has progressively increased in borehole DA-SD2 and the maximum ALT reached at the end of summer (between late August and late September), despite the ZC persisting throughout a large part of the year at the ice-rich layer (2.7 m). Maximum ALT was reached in 2022 (3.65 m). In contrast to rock wall permafrost, ALT was not reversible in the ice-rich ground of DA-SD2: for example, ALT decreased during the colder summer of 2021 at rock wall sites but not at DA-SD2 (Figure 8). At DA-SD2, ZC persisted during 2019–2021 at 2.7 m depth, and the short peak of 0°C temperature in February 2020 reaching 3.7 m depth suggests that water flowed downward (see also Phillips et al.[53]).

At DA-SD1 ALT was also stable between 2010 and 2014, with values at 2.4 m, but the lowest ALT was registered in 2019. In contrast to DA-SD2, no ZC was visible at the top of permafrost, but a small ZC can be detected at ~2.6 m (Figure S3). Only extremely limited surface subsidence (a few centimeters at most) was measured at borehole tops meaning that the ALT values was not affected as the change remained within the range of uncertainty in ALT value (Figure 7). The years with the lowest ALT at DA-SD1 (2013, 2018, and 2019) were those with the greatest snow thickness recorded at Besse (Figure 4i). Long-lasting snow cover may thus explain this unique ALT trend. The year 2019 was also where the near-surface ZC started the latest (Figure 6a).

Over the period 2010–2020, the average ALT at DA-SD2 and DA-SD1 was at 3.1 and 2.3 m depth, respectively. Maximum ALT was reached on average on 23 July at DA-SD2, and 22 August at DA-SD1.

At Aiguille du Midi, maximum ALT obviously depends on sun-exposure (Figures 7 and S3). Over the years 2010–20, it was 6.2 m on average at ADM-S, 3.5 m at ADM-NE, and 2.2 m at ADM-NW. All boreholes experienced their shallowest ALT in 2014 (1.3, 2.0, and 4.8 m for ADM-NW, ADM-NE and ADM-S respectively) which was the coldest and wettest summer at Chamonix (Figure 4e,f), while the greatest ALT was recorded in 2022 (2.7, 4.9, and 7.6 m), which was the warmest summer. However, Aiguille du Midi is the only site that directly reacted to the cold and wet summer of 2014: boreholes at the Deux Alpes may have been under rain, while under snow at Aiguille du Midi (see Section 6). At ADM-NE and ADM-NW, maximum ALT occurred at the end of the summer (on 28 August and 8 September on average, respectively), against 18 October on average at ADM-S.

Within the reference decade, ADM-S and ADM-NE have experienced the greatest ALT increase, reaching up to 2 m, while DA-SD1 ALT decreased by 0.8 m (Figure 7). Only the trend at ADM-NW was not significant ($p = .056$).

At AGM-S, ALT was in the range of ADM-NW despite having the highest surface temperature recorded within the four boreholes of the Mont Blanc Massif (Figure 5a,b). Maximum ALT is reached at a similar period as ADM-NE and ADM-NW, but the greatest ALT value was reached in 2021 (2.95 m) despite being very similar to the other years (<0.2 m difference). The coarse blocks at the near surface of AGM-S acted as a buffer and clearly dampened thaw penetration.

5.4 | Mean annual active layer thickness

MAALT is also strongly variable from one borehole to another and was not systematically consistent with ALT trends (Figure 9). For example,

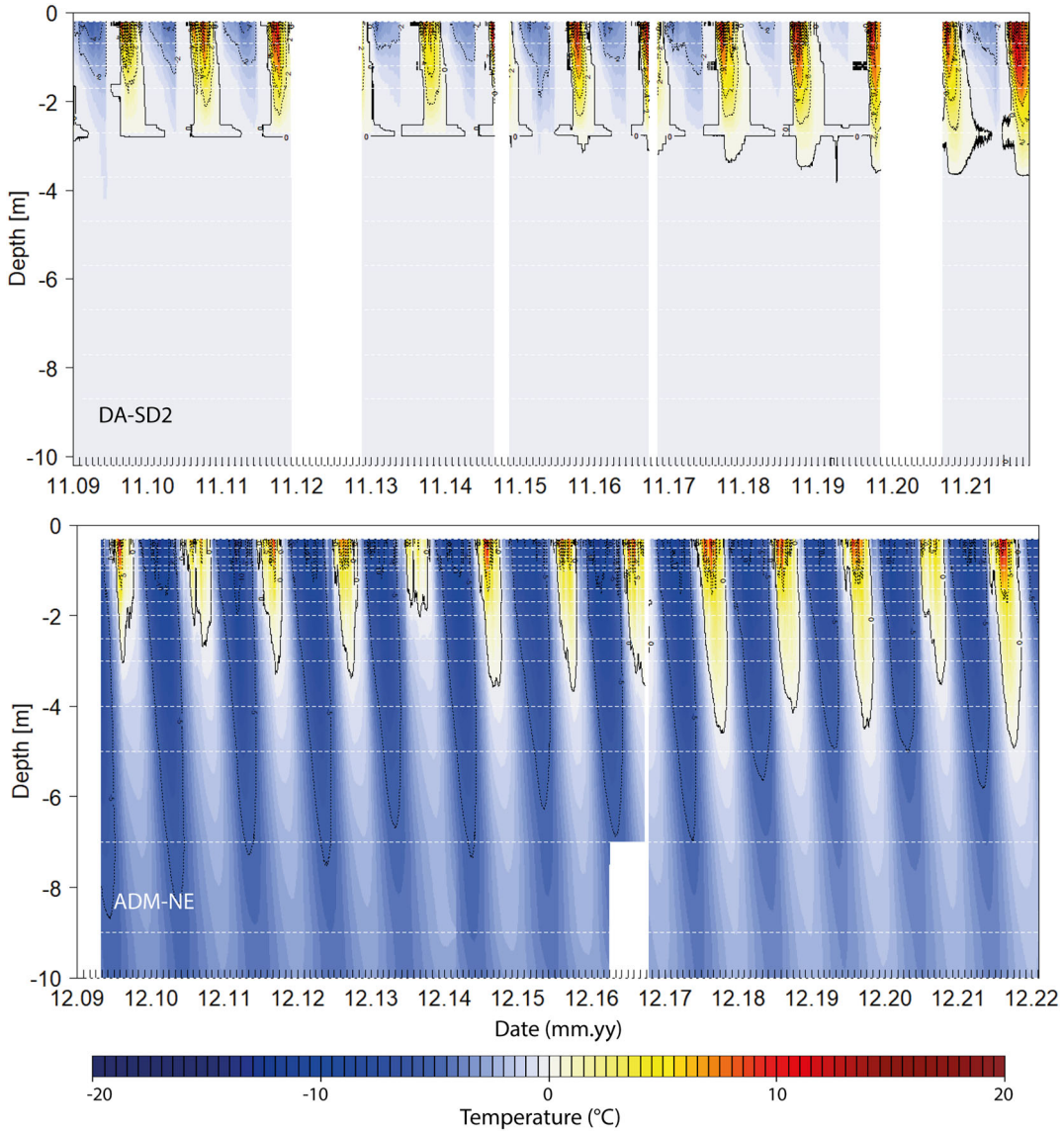

FIGURE 8 Example of the thawing season evolution displayed through daily temperature evolution in ice-rich (DA-SD2) and ice-poor (ADM-NE) permafrost sites. ALT is delineated by the 0°C isotherm (black line). A possible error in ALT due to linear interpolation between sensors is visible through the white dotted lines displaying sensor depths. Similar graphs for other boreholes are given in Figure S3. [Colour figure can be viewed at wileyonlinelibrary.com]

MAALT at ADM-S did not depict the two contrasting summers of 2014 and 2015. However, the cold summer of 2014 has marked MAALT at ADM-NE and ADM-NW. MAALT in 2022 was particularly deep at ADM-NE and ADM-S, but not at ADM-NW, and in the same range as for 2018 at ADM-NE and as for 2020 at ADM-S, despite a smaller ALT in these years. At AGM-S, MAALT remained relatively stable over the period 2018–2022, in accordance with ALT (Figure 7).

Interestingly, MAALT was reversible at DA-SD2, in contrast to ALT (Section 5.3). Indeed, MAALT almost doubled in 2019 compared to 2018, in relation to the duration of the thawing season when temperature at 0°C persisted throughout the year at the maximum thawing depth (Figure 8). Additionally, in 2020, MAALT decreased despite remaining 0.2 m greater than in the first years of monitoring and despite similar ALT as in 2019. This is due to the shorter thawing season.

5.5 | Permafrost temperature and evolution

Temperature at 10 m depth (Figure 10) shows warm and cold permafrost (i.e., >−2°C and <−2°C, respectively) in agreement with the surface temperature (Figure 5). No seasonal oscillation is visible through the 31-day running means at the two boreholes drilled in rock glaciers (DA-SD2 and DA-SD1), and no significant decrease or increase could be found at 10 m depth: the thick overlying ice-rich core of the rock glacier prevents any temperature variation.

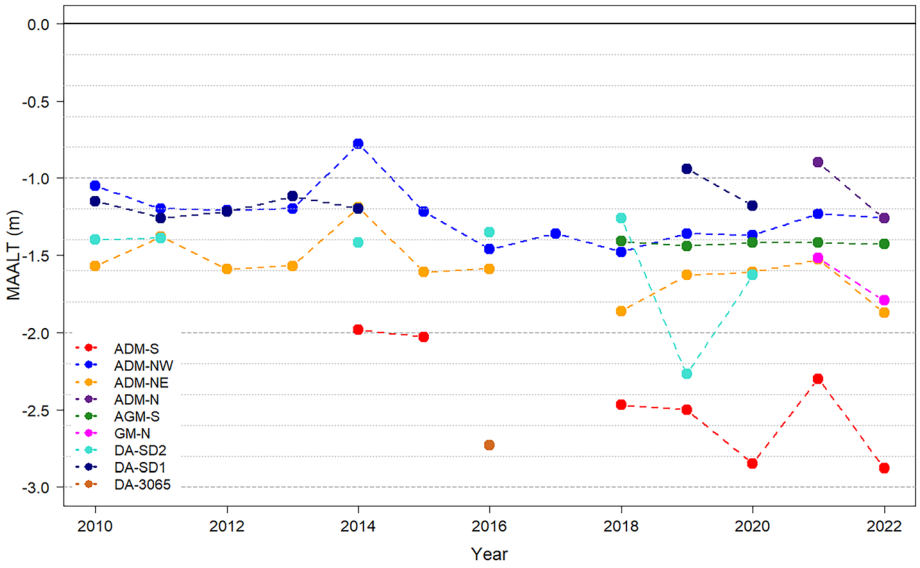

FIGURE 9 Mean annual active layer thickness (MAALT) for the available years. [Colour figure can be viewed at wileyonlinelibrary.com]

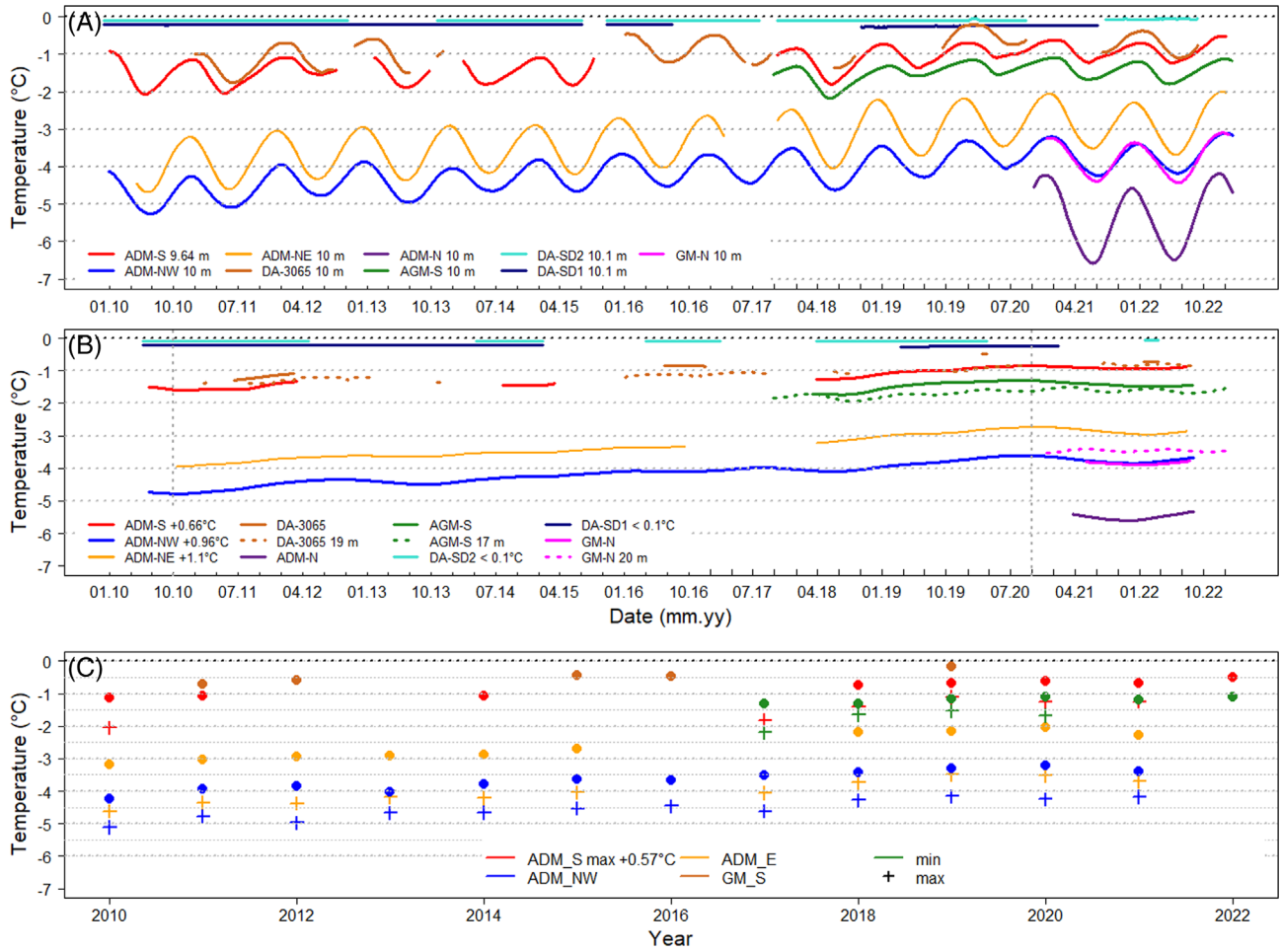

FIGURE 10 Permafrost temperature evolution: (a) at 10 m depth with a 31-day running mean; (b) at 10 m depth and between 17 and 20 m depth (dotted lines) with a 365-day running mean and 31-day running mean, respectively; and (c) minimum and maximum daily temperature registered at 10 m depth. Ten-year trend values are noted in (b) and (c) where possible. [Colour figure can be viewed at wileyonlinelibrary.com]

Seasonal oscillations were visible for all other boreholes. As for ALT, the temperature at 10 m depth increased strongly in cold and ice-poor boreholes over the reference decade (Figure 10a,b). The slope of linear regressions over the reference decade indicates a warming of up to +1.1°C at ADM-NE. ADM-S displayed the highest temperature at 10 m depth in the Mont Blanc Massif with oscillations

around −2 to −1°C but experienced the smallest temperature increase of the ADM boreholes. AGM-S displayed slightly lower temperature than ADM-S at 10 m depth with a similar thermal amplitude: coarse blocks in its near surface had a cooling effect on the ground. For ADM-NE and ADM-NW, the maximum temperature at 10 m depth has increased more than the minimum temperature, while this is the opposite of that seen at ADM-S (Figure 10c). However, at ADM-S, the trend of minimum temperature had no statistical significance ($p > .1$).

At DA-3065, a temperature increase at 10 and 19 m deep is visible despite long gaps (trend calculated over an 8-year period: 2012–2019); the maximum temperature has increased less than the average based on the 365-day running mean—similarly to ADM-S, the other warm bedrock permafrost.

5.6 | Temperature–depth profiles

Figure 11 shows Tz (temperature–depth) profiles of mean annual temperature (hydrological years), down to a depth of 10 m to allow comparison between boreholes. Tz profiles for boreholes extending at a greater depth are reported in Figure S4. For DA-SD1 and DA-SD2 (Figure 11f,g), permafrost temperature showed almost no change below 4 m depth over the decade. Seasonal and interannual oscillations were blocked at the top of the ice-rich permafrost core, which can be considered as the ZAA. These two boreholes can be considered as isothermal down to the underlying bedrock (9.5–13.5 m), and their temperature very close to 0°C raises the question of the melting point temperature and thus mineralization of the ice. DA-SD2 experienced a strong warming down to 4 m depth in 2019 while this warming reached 2 m depth at DA-SD1. In 2015, a cold anomaly at 6.6 m depth at DA-SD1 might be due to internal air circulation in porosities (chimney effect) when positive temperature started at the surface in summer.[54] This interpretation is suggested by the coincidence between the initiation of cooling at 6.6 m depth with surface thawing for several years (Figure S5), which thus allows air to circulate. Furthermore, cooler conditions in 2012 and 2014 between 2 and 4 m depth are possibly due to sensor drifting (see also Figures S3 and S4).

For all other boreholes, temperature increased steadily from year to year at all depths down to 10 m, with 2011 being the coldest year, while the warmest year was 2020 or 2022, depending on borehole, except at the near-surface of AGM-S and DA-SD2 where 2019 was slightly warmer (2022 data not available for this last borehole). At ADM-NW (Figure 11a), the shape of the profiles was strongly influenced by local snow accumulation at the surface and by an open fracture at 2.5 m depth which locally cooled the rock[47]: a combination of snow insulation and air ventilation effects caused strong negative gradients near the surface. Nevertheless, the local cold distortion at 2.5 m was less visible in 2020 and 2022, the two warmest years. Unlike ADM-NW, the snow-free ADM-N (Figure 11d) was not affected by a local snow effect and showed colder near-surface conditions (<−5°C).

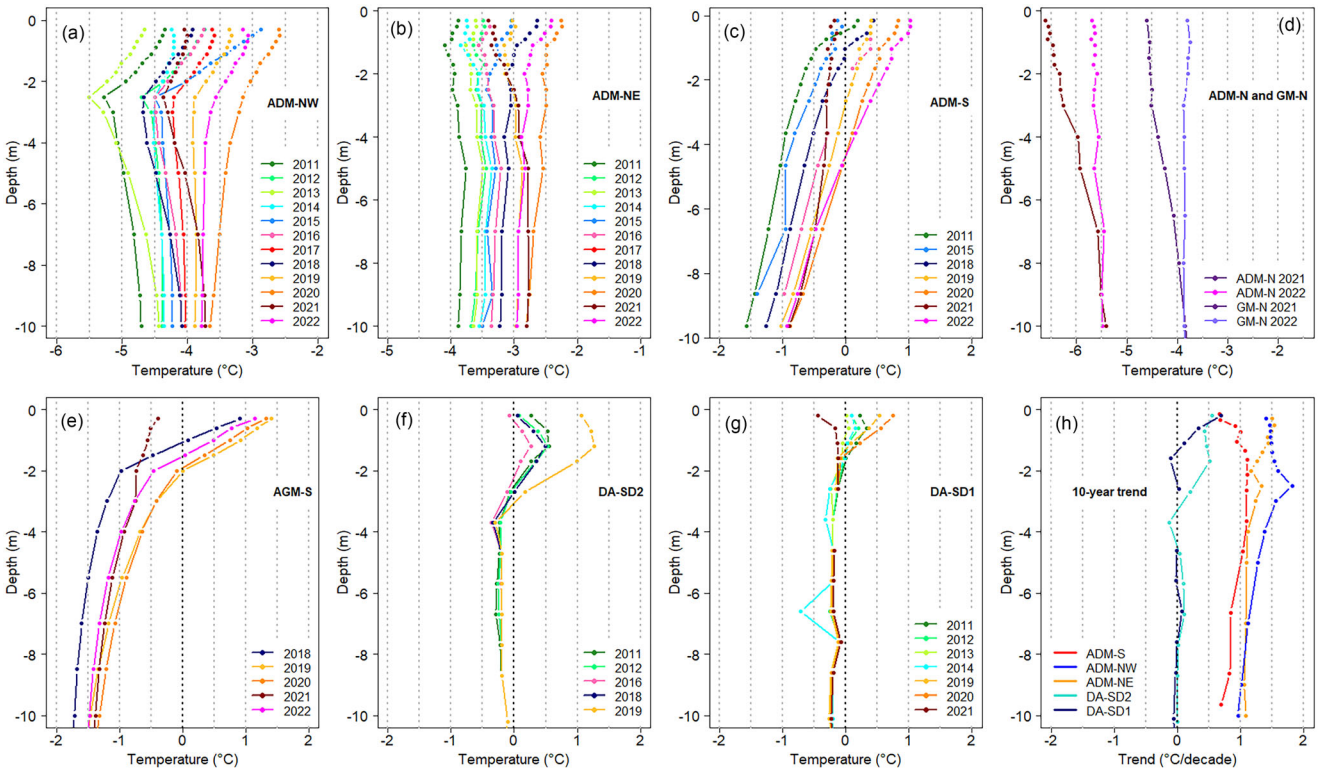

FIGURE 11 (a–g) Mean annual temperature–depth (Tz) profiles; (h) linear trend calculated with the annual values along Tz profiles for the reference decade 2011–2020. [Colour figure can be viewed at wileyonlinelibrary.com]

At AGM-S (Figure 11e), the Tz profile shape confirmed the interpretation of the surface and 10 m depth temperature trend: the upper 2 m showed a strong temperature gradient revealing a very low-conductivity layer[52] that corresponds to the coarse blocks cooling the ground, while the steeper profile below 2 m depth depicted a higher-conductivity layer corresponding to the bedrock (Figure 11c).

Focusing on the 10-year change (Figure 11h), the upper 2 m of DA-SD1 and DA-SD2 hase experienced a positive trend up to 1°C, respectively, while temperature remained stable deeper. Data that are difficult to interpret at DA-SD1 (see Figures S3 and S4) have been removed to calculate this trend. For the ADM boreholes, Tz profiles have increased by 0.5°C to nearly 2°C. The strongest increase was at around the 2.5-m-deep open fracture at ADM-NW. Immediately below the fracture, the temperature increase was 1.5°C; it lowered steadily to a depth of 10 m to almost 1°C. This 1°C increase was also found between 2 and 4 m depth at ADM-S, and from 4 to 10 m depth at ADM-NE. A profile distortion was also visible at 2.5 m depth of ADM-NE and may reflect a fracture effect. Note that at ADM-S, the surface sensors indicated a stronger increase in the 365-day running mean (Figure 5b) than the linear trend calculated here based on the annual average (Figure 11f).

Four DTS measurements with an optic fiber at DA-3065 in 2013 indicate that the ZAA is between 25 and 30 m depth (Figure 12a). Comparison with the sensor temperatures in this borehole for the same days of 2013 (Figure 12b–e) shows that sensors at 44, 59, 69, 94, and 99 m depth were not reliable and should not be interpreted as indicating taliks. Sensors at 79 and 89 m were within cumulative calibration and measurement errors with DTS measurements except in July 2013. Therefore, DTS measurements were the most reliable method for depths below 40 m and show a gradient of permafrost temperature from −1.3°C at 40 m to −0.8 at 98 m.

6 | DISCUSSION

The *PermaFrance* network has provided usable decadal time series despite the difficulties in ensuring their continuity. Gaps in the time series are more frequent in flat or gently inclined terrains (Deux Alpes boreholes, Figure 2) due to water infiltration during snow melt or heavy spring rain on to snow, in addition to battery exhaustion and lightning strikes.[50] Furthermore, in this type of ground it is sometimes difficult to distinguish effects of possible natural processes (air circulation) from sensor drift or failure.

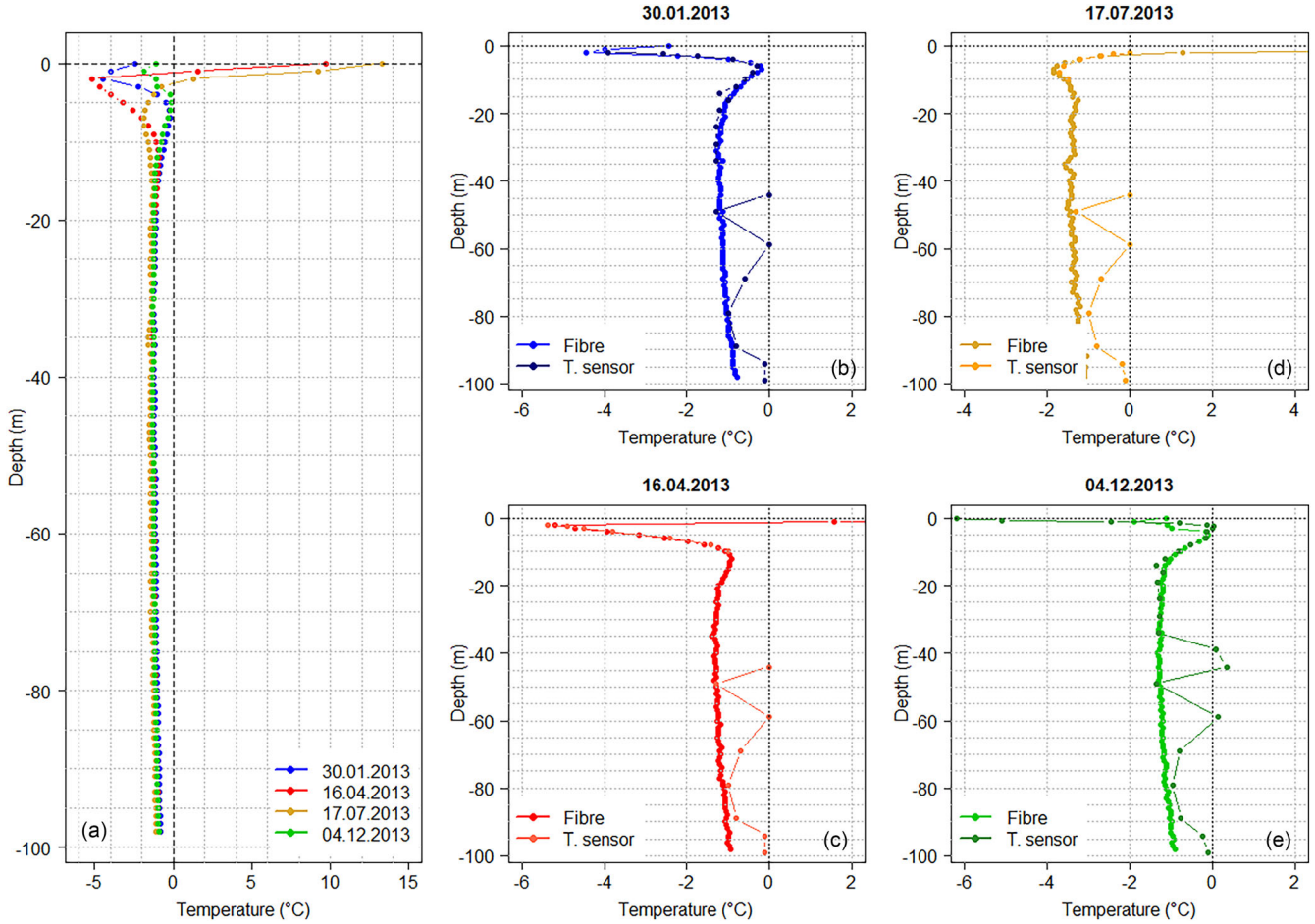

FIGURE 12 DA-3065 borehole: (a) four DTS measurements in 2013; (b–e) comparison of DTS measurements with sensor temperature. Unreliable sensors at 40, 45, 60, 70, 95, and 99 m appear as clear outliers. [Colour figure can be viewed at wileyonlinelibrary.com]

The measured permafrost temperature shows high variability both on a regional scale and within a single site. Despite the short monitoring period, the results highlight the importance of local conditions such as ground type (bedrock vs. rock glacier), porosity, ice content, snow cover, and sun-exposure. This local dependence on ground characteristics is also true for Arctic permafrost (e.g., Romanovsky et al.[32]) but alpine topography considerably modulates the energy balance causing a high level of spatial variability.[55] In the *PermaFrance* data, elevation and sun-exposure explain the permafrost type (cold vs. warm): cold permafrost is found only in the most shaded exposures and above 3500 m. At a finer scale, comparison of ADM-S with AGM-S shows that a near-surface layer of coarse blocks also affects the thermal regime: AGM-S is ~0.5°C colder than ADM-S at 10 m depth despite (Figure 10) a lower elevation and a higher surface temperature. Convection in the coarse blocks probably results in cooling of the ground.[54]

However, permafrost evolution depends on ground characteristics. Temperature trends at 10 m depth depict strong contrasts between warm ice-rich and cold ice-poor permafrost: a warming is observed in all boreholes except the two warm ice-rich boreholes of Bellecombe rock glacier (Deux Alpes). In the cold east and NW faces of the Aiguille du Midi, some of the strongest temperature increases (>1°C per decade) in the world have been registered and are in the range of those at Janssonhaugen in Svalbard.[28] Although direct comparison is limited by the slight time lag of the reference periods, we note that this increase is slightly greater than the temperature increase observed at 10 m depth at the Jungfrau East ridge between 2009 and 2019 (+0.8°C), which is the most pronounced warming reported in Switzerland.[29] 3D heat fluxes in alpine rock walls reinforce temperature change at depth[56] and the topoclimatic control may partly explain this enhanced response to air temperature increase. At ADM-S, the entirety of this warming has not yet reached 10 m. The ~1°C increase is found from 2 to 4.5 m depth, which can be attributed to the delayed response to air temperature because of latent heat uptake at this warm permafrost site.[52] For the ice-poor warm permafrost boreholes recording temperature evolution at 10 m depth (AGM-S, ADM-S, and DA-3065), minimum values increased more than the average and maximum temperatures, suggesting a response to air temperature increase during winter and a dampened reaction to summer heat that can also be attributed to latent heat uptake during the thawing period. Finally, at warm, ice-rich permafrost sites (DA-SD1 and DA-SD2) latent heat consumption for ice melting negates any short-term response of permafrost to air temperature increase. For these sites, temperature changes are predominately observed within the active layer whose maximum thicknesses also marks the ZAA.

ALT increase since 2015 and especially since 2018, coincides with higher summer air temperatures (Figure 4e). Thus, summer 2015 marks a turning point in ALT regime with consistent increase in maximum ALT from that summer in all boreholes except at DA-SD1, independently of their ice content. This has also been observed in Switzerland, where significant subsurface ice melting[57] and rock glacier acceleration[29] were reported in 2015. However, ALT in 2015 in the Swiss Alps was not greater than during the summer 2003 heat wave.[29] Therefore, this consistent ALT increase since 2015 may not be irreversible, especially at ice-poor sites. However, the intensity of thawing as depicted by MAALT has a more chaotic pattern and, in contrast to ALT, shows reversibility in ice-rich ground.

The summer of 2022, which experienced particularly high air temperatures, has resulted in an obvious ALT increase in some boreholes (ADM-NE, ADM-S, DA-SD2), but in some others, it was not thicker than in 2020 or remained within the uncertainty range (AGM-S, ADM-NW). Focusing on the period 2019–2021, it is interesting to note that ALT was generally greater in 2020 in rock wall sites (ADM), despite a cooler summer than in 2019 (Figure 4e). Snow melt was earlier than the two other years in the Mont Blanc Massif (Figure 4i) and positive surface temperature occurred much earlier in 2020 than in 2019 (Figure 6b,c): early snow melting favoring early active layer thawing may explain this greater ALT in 2020, which is in agreement with former modeling studies.[45] Conversely, at the Deux Alpes boreholes, snow lasted longer in 2020 than in 2019 (Figure 6a) but ALT also increased in 2020 compared to 2019 at DA-SD1 and DA-SD2. The timing of snow melting could have different impacts in porous ground allowing snow melt water infiltration[58] than in impermeable bedrock. Nevertheless, the opposite trend of ALT at DA-SD1 can only be explained by a snow cover effect and shows a possible local effect of the persistence of snow patches during summer. Such a local snow effect on ALT is often observed in polar environments (e.g., Strand et al.[59]) and was also noted from surface temperature measurements in mountain permafrost conditions.[60]

In contrast to the ADM boreholes, ALT also increased in 2021 at DA-SD2 despite being the coldest summer since 2016. This highlights a possible cumulative effect of repeated hot summers favoring interstitial ice erosion and a deeper penetration of the heat from one year to another. This interpretation is supported by the observation of moderate surface subsidence that indicates probable ice loss at the permafrost table. The surface subsidence should be subtracted from the measurement to get true ALT, but subsidence is in the range of the ALT interpolation uncertainty.

At very high elevation (~>3500 m), snow falls all year long, and the smaller ALT observed in 2014 at the high-elevation Aiguille du Midi boreholes but not in the less elevated Deux Alpes boreholes suggests that summer snow fall could strongly impact ALT. Summer 2014 was particularly cold, but not colder than 2011 (Figure 4e), and was also particularly wet (Figure 4f). At Aiguille du Midi, air temperature was rarely >0°C (Figure 13a), and precipitation may have thus fallen as snow, protecting the rock from direct solar radiation, while it was more likely rain at the Deux Alpes boreholes (Figure 13b). Beyond the ALT and surface temperature, snow control on permafrost temperature is difficult to decipher.

At the surface, snow-poor sites experienced the greatest temperature increase. The same pattern was also found in some Arctic sites where ALT increase is greater at snow-poor sites that are more coupled with winter air temperature increases.[34,59] Rock wall surface warming can even exceed that of air temperature, probably because of the effect of direct solar radiation.[61,62] Since snow may last during

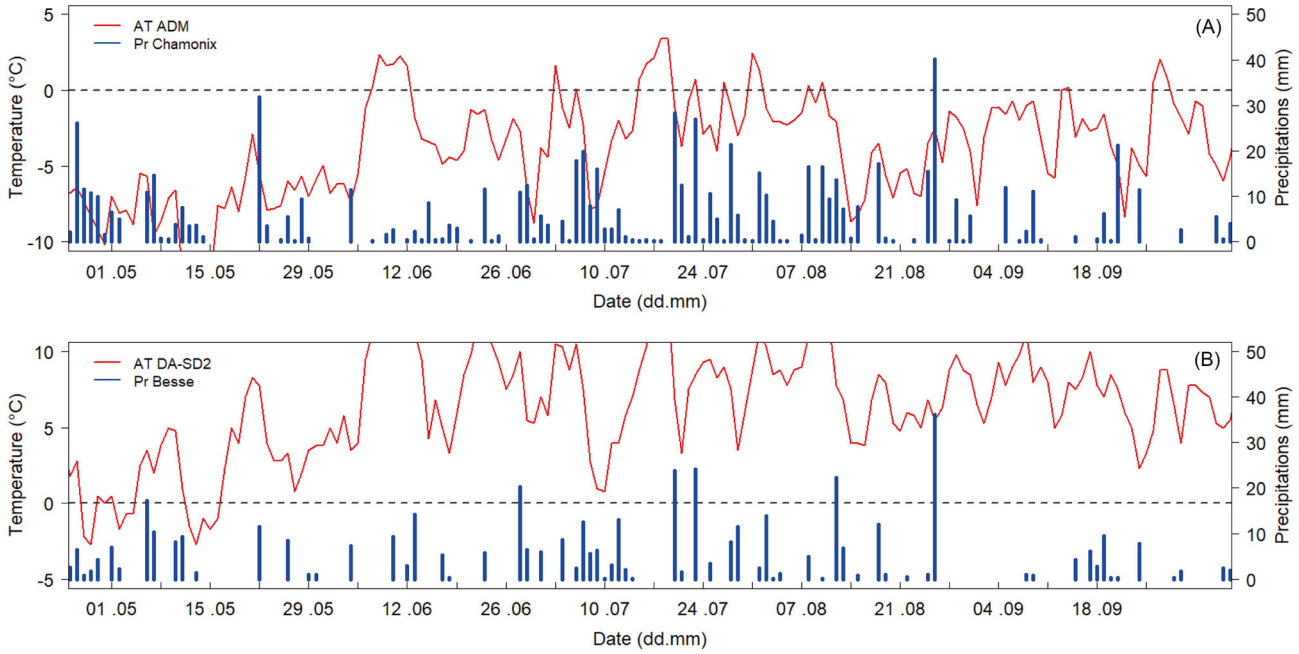

FIGURE 13 Precipitation and air temperature during summer 2014 in (a) the Mont Blanc Massif—air temperature was available during this period at the top of the AdM (*Météo France* data) and have been adjusted to the lowest borehole elevation by using a standard lapse rate of 0.55°C/100 m; and (b) the Ecrins Massif—air temperature was extrapolated at the elevation of the Deux Alpes boreholes from Besse weather station using the same lapse rate as for the Mont Blanc Massif. [Colour figure can be viewed at wileyonlinelibrary.com]

spring and early summer while direct solar radiation is high, surface warming is reduced at snow-covered sites, counterbalancing the winter insulation effect.[45] Similarly to previously published data, the variability in snow cover dynamics may also lead to variable surface temperature trends.[28,34]

7 | CONCLUSION AND OUTLOOKS

In the French Alps, permafrost temperatures have been measured since 2010 in nine boreholes 10–100 m deep, drilled at sites with varying topography and ground conditions. Analysis of temperature records (up to 12 years) indicates important intraregional and local variability in permafrost conditions and evolution. The main conclusions are:

- The 2010–2022 measurement period coincides with the highest atmospheric temperature since at least 1981 while no major change has been observed in precipitation. During the 2011–2020 reference decade, winter and summer experienced significant warming (up to +3.65°C in winter) but spring and fall did not change appreciably. Precipitation has increased slightly in winter and decreased in summer.
- Comparison of the thermal state recorded in the nine boreholes shows variable permafrost conditions from very cold to isothermal and close to 0°C conditions. These permafrost conditions depend mostly on elevation and sun-exposure whereas permafrost evolution depends on permafrost type (warm vs. cold), ice-content, and ground surface characteristics.
- The near-surface temperature increase is more pronounced at snow-free sites (rock walls) where it can exceed that of air temperature, than at snow-covered sites where it is two to four times lower than that of the air.
- ALT has increased in all boreholes except one, with linear trends reaching +2 m over the 2011–2020 decade in both cold and warm rock wall permafrost. One borehole in Bellecombe rock glacier at the Deux Alpes (DA-SD1) showed a decreasing ALT trend which could be attributed to local snow effects, while the nearby DA-SD2 had an increasing ALT trend. These contrasting trends within a footprint have also been found in other mountainous and polar areas.
- Since 2015, a significant shift in maximum ALT regime has been detected for all boreholes with decadal times series except DA-SD1, independently of their ice content and thermal state, in relation with warmer summers. Although 2022 was the warmest summer, ALT did not increase in all boreholes. At AGM-S, ALT remained remarkably stable during the period 2018–2022, probably because of the dampening effect of coarse block cover. Moreover, the intensity of thaw (MAALT) did not show such a systematic deepening over the reference decade, although it increased in a minority of boreholes for some years.
- ALT increase was reversible in the rock wall but not at the ice-rich DA-SD2 where the durable ZC at the permafrost table underlines the role of progressive ice melting in ALT evolution. Prior to 2015,

melting ice clearly prevented an ALT increase, but ALT began to increase gradually from 2015 onward, suggesting that ice at the permafrost table partially melted, allowing heat to propagate into deeper layers from one year to the next. The ALT increase is less reversible for this ground type, unlike MAALT.

- Snow has also played a significant role in ALT trends at rock wall sites: early snow melt in spring favors ALT increase in rock wall sites consistent with earlier positive temperatures. At debris sites, infiltration of snowmelt water could counteract the effect of sustained sub-zero temperatures at the surface caused by snow.
- There is a clear distinction in the temperature trend between close to 0°C ice-rich and ice-poor permafrost, the former displaying no change over 10 years while the latter recording one of the greatest permafrost warmings reported worldwide (>+1°C) within recent decades. This remarkable warming only reached 4.5–5 m depth at warm permafrost rock walls (ADM-S) as its propagation is delayed by latent heat consumption.
- 2020 and 2022 were the warmest years recorded in almost all boreholes except at AGM-S where 2019 was slightly warmer than 2020 down to 2.5 m and 2022 was even colder than 2021 down to 17 m depth, suggesting the combined effect of latent heat consumption and dampening from the coarse block layer.

In addition to these main results, this study also points to the difficulty to ensuring continuous permafrost monitoring in remote and harsh mountain areas.[34] It furthermore highlights the importance of long-term monitoring over several decades as reported by other studies (e.g., Haberkorn et al.[29]). Substantial means in terms of staff, equipment and fundings are thus required to maintain these installations and ensure long-term monitoring. Finally, the wide disparity in thermal state and trends of permafrost in high-mountain environments highlights the need (a) to monitor in variable conditions and places, and (b) to develop physically based investigation to better decipher the respective role of snow parameters (thickness, duration, period of melting), ice ground type (ice-rich, ice-poor, water/ice ratio), and solar radiation.

ACKNOWLEDGEMENTS

The authors acknowledge the 'Commission observation' of the Observatoire des Sciences de l'Univers de Grenoble (OSUG) and the various projects that funded the installation and equipment (EU POIA PermaRisk, EU Alpine Space PermaNET, EU Alcotra PrévRisk Haute Montagne). The authors are also very grateful to the *Compagnie du Mont Blanc*, the *Société des Téléphériques de la Grande Motte*, and *Deux Alpes Loisirs* for access to monitoring sites. They furthermore acknowledge the anonymous reviewers and editor Mauro Guglielmin for constructive comments on the manuscript and Catherine Simpson for improving the English text.

DATA AVAILABILITY STATEMENT

Data are available via the GTN-P portal: https://gtnp.arcticportal.org/.

ORCID

Florence Magnin https://orcid.org/0000-0002-0734-7459
Xavier Bodin https://orcid.org/0000-0001-6245-4030

REFERENCES

1. WMO. The global observing system for climate: implementation needs. 2016. https://library.wmo.int/doc_num.php?explnum_id=3417
2. Vonk JE, Gustafsson Ö. Permafrost-carbon complexities. *Nat Geosci*. 2013;6(9):675-676. doi:10.1038/ngeo1937
3. Hjort J, Streletskiy D, Doré G, Wu Q, Bjella K, Luoto M. Impacts of permafrost degradation on infrastructure. *Nat Rev Earth Environ*. 2022;3(1):24-38. doi:10.1038/s43017-021-00247-8
4. Berthling I, Etzelmüller B. The concept of cryo-conditioning in landscape evolution. *Quatern Res*. 2011;75(2):378-384. doi:10.1016/j.yqres.2010.12.011
5. Lantuit H, Overduin PP, Wetterich S. Recent Progress regarding permafrost coasts. *Permafr Periglac Proces*. 2013;24(2):120-130. doi:10.1002/ppp.1777
6. Lewkowicz AG, Way RG. Extremes of summer climate trigger thousands of thermokarst landslides in a High Arctic environment. *Nat Commun*. 2019;10:1329. doi:10.1038/s41467-019-09314-7
7. Luo J, Niu F, Lin Z, Liu M, Yin G. Recent acceleration of thaw slumping in permafrost terrain of Qinghai-Tibet Plateau: an example from the Beiluhe Region. *Geomorphology*. 2019;341:79-85. doi:10.1016/j.geomorph.2019.05.020
8. Allen S, Frey H, Haeberli W, Huggel C, Chiarle M, Geertsema M. Assessment principles for glacier and permafrost hazards in mountain regions. 2022. doi:10.1093/acrefore/9780199389407.013.356
9. Deline P, Gruber S, Amann F, et al. Chapter 15—ice loss from glaciers and permafrost and related slope instability in high-mountain regions. In: Haeberli W, Whiteman C, eds. *Snow and Ice-Related Hazards, Risks, and Disasters*. Second ed. Elsevier; 2021:501-540. doi:10.1016/B978-0-12-817129-5.00015-9
10. Haeberli W, Schaub Y, Huggel C. Increasing risks related to landslides from degrading permafrost into new lakes in de-glaciating mountain ranges. *Geomorphology*. 2017;293:405-417. doi:10.1016/j.geomorph.2016.02.009
11. Hjort J, Karjalainen O, Aalto J, et al. Degrading permafrost puts Arctic infrastructure at risk by mid-century. *Nat Commun*. 2018;9(1):5147. doi:10.1038/s41467-018-07557-4
12. Ravanel L, Magnin F, Deline P. Impacts of the 2003 and 2015 summer heatwaves on permafrost-affected rock-walls in the Mont Blanc massif. *Sci Total Environ*. 2017;609:132-143. doi:10.1016/j.scitotenv.2017.07.055
13. Ravanel L, Deline P. Climate influence on rockfalls in high-Alpine steep rockwalls: the north side of the Aiguilles de Chamonix (Mont Blanc massif) since the end of the 'Little Ice Age'. *Holocene*. 2011;21(2):357-365. doi:10.1177/0959683610374887
14. Allen SK, Cox SC, Owens IF. Rock avalanches and other landslides in the central southern Alps of New Zealand: a regional study considering possible climate change impacts. *Landslides*. 2011;8(1):33-48. doi:10.1007/s10346-010-0222-z
15. Walter F, Amann F, Kos A, et al. Direct observations of a three million cubic meter rock-slope collapse with almost immediate initiation of ensuing debris flows. *Geomorphology*. 2020;351:106933. doi:10.1016/j.geomorph.2019.106933
16. Bodin X, Krysiecki J-M, Schoeneich P, et al. The 2006 collapse of the Bérard rock glacier (Southern French Alps). *Permafr Periglac Proces*. 2017;28(1):209-223. doi:10.1002/ppp.1887
17. Marcer M, Serrano C, Brenning A, Bodin X, Goetz J, Schoeneich P. Evaluating the destabilization susceptibility of active rock glaciers in the French Alps. *Cryosphere*. 2019;13(1):141-155. doi:10.5194/tc-13-141-2019

18. Marcer M, Nielsen SR, Ribeyre C, et al. Investigating the slope failures at the Lou rock glacier front. *French Alps Permafr Periglac Proces*. 2020;31(1):15-30. doi:10.1002/ppp.2035
19. Marcer M, Cicoira A, Cusicanqui D, et al. Rock glaciers throughout the French Alps accelerated and destabilised since 1990 as air temperatures increased. *Communic Earth Environ*. 2021;2(1):1-11. doi:10.1038/s43247-021-00150-6
20. Bodin X, Schoeneich P, Deline P, et al. Mountain permafrost and associated geomorphological processes: recent changes in the French Alps. *J Alpine Res Revue de Géographie Alpine*. 2015;(103-2):103-102. doi:10.4000/rga.2885
21. Duvillard P-A, Ravanel L, Schoeneich P, Deline P, Marcer M, Magnin F. Qualitative risk assessment and strategies for infrastructure on permafrost in the French Alps. *Cold Reg Sci Technol*. 2021;189:103311. doi:10.1016/j.coldregions.2021.103311
22. Duvillard P-A, Ravanel L, Deline P. Risk assessment of infrastructure destabilisation due to global warming in the high French Alps. *J Alpine Res Revue de Géographie Alpine*. 2015;(103-2):1-15. doi:10.4000/rga.2896
23. Duvillard P-A, Ravanel L, Marcer M, Schoeneich P. Recent evolution of damage to infrastructure on permafrost in the French Alps. *Reg Environ Change*. 2019;19(5):1281-1293. doi:10.1007/s10113-019-01465-z
24. Mourey J, Marcuzzi M, Ravanel L, Pallandre F. Effects of climate change on high Alpine mountain environments: evolution of mountaineering routes in the Mont Blanc massif (Western Alps) over half a century. *Arctic, Antarctic, Alpine Res*. 2019;51(1):176-189. doi:10.1080/15230430.2019.1612216
25. Mourey J, Lacroix P, Duvillard P-A, et al. Rockfall and vulnerability of mountaineers on the west face of the Aiguille du Goûter (classic route up Mont Blanc, France), an interdisciplinary study. *Natural Hazards Earth Syst Sci Discus*. 2021;1-29. doi:10.5194/nhess-2021-128
26. Biskaborn BK, Lanckman J-P, Lantuit H, et al. The new database of the Global Terrestrial Network for Permafrost (GTN-P). *Earth Syst Sci Data*. 2015;7(2):245-259. doi:10.5194/essd-7-245-2015
27. Christiansen HH, Etzelmüller B, Isaksen K, et al. The thermal state of permafrost in the nordic area during the international polar year 2007–2009. *Permafr Periglac Proces*. 2010;21(2):156-181. doi:10.1002/ppp.687
28. Etzelmüller B, Guglielmin M, Hauck C, et al. Twenty years of European mountain permafrost dynamics—the PACE legacy. *Environ Res Lett*. 2020;15(10):104070. doi:10.1088/1748-9326/abae9d
29. Haberkorn A, Kenner R, Noetzli J, Phillips M. Changes in ground temperature and dynamics in mountain permafrost in the Swiss Alps. *Front Earth Sci*. 2021;9:1-21. doi:10.3389/feart.2021.626686
30. Harris C, Haeberli W, Vonder Mühll D, King L. Permafrost monitoring in the high mountains of Europe: the PACE project in its global context. *Permafr Periglac Proces*. 2001;12(1):3-11. doi:10.1002/ppp.377
31. PERMOS. Permafrost in Switzerland, 2014/2015 to 2017/2018 (Glaciological Report Permafrost No. 16–19) (p. 104). Commission of the Swiss Academy of Sciences. 2019. doi:10.13093/permos-rep-2019-16-19
32. Romanovsky VE, Smith SL, Christiansen HH. Permafrost thermal state in the polar Northern Hemisphere during the international polar year 2007–2009: a synthesis. *Permafr Periglac Proces*. 2010;21(2):106-116. doi:10.1002/ppp.689
33. Biskaborn BK, Smith SL, Noetzli J, et al. Permafrost is warming at a global scale. *Nat Commun*. 2019;10(1):264. doi:10.1038/s41467-018-08240-4
34. Smith SL, O'Neill HB, Isaksen K, Noetzli J, Romanovsky VE. The changing thermal state of permafrost. *Nat Rev Earth Env*. 2022;3(1):10-23. doi:10.1038/s43017-021-00240-1
35. Schoeneich P, Bodin X, Krysiecki J-M, Deline P, Ravanel L. *Permafrost in France. PermaFrance network, report n° 1*. Institut de Géographie Alpine; 2010. 74 pp
36. Durand Y, Laternser M, Giraud G, Etchevers P, Lesaffre B, Mérindol L. Reanalysis of 44 Yr of climate in the French Alps (1958–2002): methodology, model validation, climatology, and trends for air temperature and precipitation. *J Appl Meteorol Climatol*. 2009;48(3):429-449. doi:10.1175/2008JAMC1808.1
37. Marcer M, Bodin X, Brenning A, Schoeneich P, Charvet R, Gottardi F. Permafrost favorability index: spatial modeling in the French Alps using a rock glacier inventory. *Front Earth Sci*. 2017;5:1-17. doi:10.3389/feart.2017.00105
38. Gardent M, Rabatel A, Dedieu J-P, Deline P. Multitemporal glacier inventory of the French Alps from the late 1960s to the late 2000s. *Global Planet Change*. 2014;120:24-37. doi:10.1016/j.gloplacha.2014.05.004
39. Durand Y, Giraud G, Laternser M, Etchevers P, Mérindol L, Lesaffre B. Reanalysis of 47 years of climate in the French Alps (1958–2005): climatology and trends for snow cover. *J Appl Meteorol Climatol*. 2009;48(12):2487-2512. doi:10.1175/2009JAMC1810.1
40. Paul F, Rastner P, Azzoni RS, et al. Glacier shrinkage in the Alps continues unabated as revealed by a new glacier inventory from Sentinel-2. *Earth Syst Sci Data*. 2020;12:1805-1821. doi:10.5194/essd-12-1805-2020
41. Davaze L, Rabatel A, Dufour A, Hugonnet R, Arnaud Y. Region-wide annual glacier surface mass balance for the European Alps from 2000 to 2016. *Front Earth Sci*. 2020;8:1-14. https://www.frontiersin.org/article/10.3389/feart.2020.00149
42. Boeckli L, Brenning A, Gruber S, Noetzli J. Permafrost distribution in the European Alps: calculation and evaluation of an index map and summary statistics. *Cryosphere*. 2012;6(4):807-820. doi:10.5194/tc-6-807-2012
43. Magnin F, Brenning A, Bodin X, Deline P, Ravanel L. Statistical modelling of rock wall permafrost distribution: application to the Mont Blanc massif. *Géomorphol: Rel Proces Environ*. 2015;20(2):145-162. doi:10.4000/geomorphologie.10965
44. Magnin F, Josnin J-Y, Ravanel L, Pergaud J, Pohl B, Deline P. Modelling rock wall permafrost degradation in the Mont Blanc massif from the LIA to the end of the 21st century. *Cryosphere*. 2017;11(4):1813-1834. doi:10.5194/tc-11-1813-2017
45. Magnin F, Westermann S, Pogliotti P, Ravanel L, Deline P, Malet E. Snow control on active layer thickness in steep alpine rock walls (Aiguille du Midi, 3842ma.s.l., Mont Blanc massif). *Catena*. 2017;149:648-662. doi:10.1016/j.catena.2016.06.006
46. Legay A, Magnin F, Ravanel L. Rock temperature prior to failure: analysis of 209 rockfall events in the Mont Blanc massif (Western European Alps). *Permafr Periglac Proces*. 2021;32(3):520-536. doi:10.1002/ppp.2110
47. Magnin F, Deline P, Ravanel L, Noetzli J, Pogliotti P. Thermal characteristics of permafrost in the steep alpine rock walls of the Aiguille du Midi (Mont Blanc Massif, 3842 m a.s.l). *Cryosphere*. 2015;9(1):109-121. doi:10.5194/tc-9-109-2015
48. Schoeneich P, Echelard T, Krysiecki J-M, et al. The borehole 2Alpes-3065—a pilot installation for fiber optic DTS measurements in permafrost. Tenth International Conference on Permafrost, June 2012, Salekhard. Vol. 4/2, Extended abstracts. 2012;507–508.
49. Schoeneich P., Krysiecki J.-M, Mingrat L, Huwald H. DTS ground temperature measurements in mountain permafrost—the 2Alpes-3065 borehole (French Alps). GeoQuebec 2015 – 7th Canadian Conference on Permafrost, September 2015, Paper n° 823, 6 p. 2015.
50. Schoeneich P, Krysiecki J-M. 2alpes-3065 – les tribulations d'un forage d'altitude. In: Monitoring en milieux naturels – Retours d'expériences en terrains difficiles. Collection EDYTEM. 2017;19(1):95–100. doi:10.3406/edyte.2017.1368
51. Hanson S, Hoelzle M. The thermal regime of the active layer at the Murtèl rock glacier based on data from 2002. *Permafr Periglac Proces*. 2004;15(3):273-282. doi:10.1002/ppp.499

52. Williams PJ, Smith MW. *The Frozen Earth: Fundamentals of Geocryology*. Cambridge University Press; 1989:306. doi:10.1017/CBO9780511564437
53. Phillips M, Haberkorn A, Draebing D, Krautblatter M, Rhyner H, Kenner R. Seasonally intermittent water flow through deep fractures in an Alpine Rock Ridge: Gemsstock, Central Swiss Alps. *Cold Reg Sci Technol*. 2016;125:117-127. doi:10.1016/j.coldregions.2016.02.010
54. Harris SA, Pedersen DE. Thermal regimes beneath coarse blocky materials. *Permafr Periglac Proces*. 1998;9(2):107-120. doi:10.1002/(SICI)1099-1530(199804/06)9:23.0.CO;2-G
55. Gruber S, Haeberli W. Mountain permafrost. In: Margesin R, ed. *Permafrost Soils*. Springer; 2009:33-44. doi:10.1007/978-3-540-69371-0_3
56. Noetzli J, Gruber S, Kohl T, Salzmann N, Haeberli W. Three-dimensional distribution and evolution of permafrost temperatures in idealized high-mountain topography. *J Geophys Res Earth*. 2007;112(F2):F02S13. doi:10.1029/2006JF000545
57. Mollaret C, Hilbich C, Pellet C, Flores-Orozco A, Delaloye R, Hauck C. Mountain permafrost degradation documented through a network of permanent electrical resistivity tomography sites. *Cryosphere*. 2019;13(10):2557-2578. doi:10.5194/tc-13-2557-2019
58. Luethi R, Phillips M, Lehning M. Estimating non-conductive heat flow leading to intra-permafrost Talik formation at the Ritigraben Rock Glacier (Western Swiss Alps). *Permafr Periglac Proces*. 2017;28(1):183-194. doi:10.1002/ppp.1911
59. Strand SM, Christiansen HH, Johansson M, Åkerman J, Humlum O. Active layer thickening and controls on interannual variability in the Nordic Arctic compared to the circum-Arctic. *Permafr Periglac Proces*. 2021;32(1):47-58. doi:10.1002/ppp.2088
60. Gubler S, Fiddes J, Keller M, Gruber S. Scale-dependent measurement and analysis of ground surface temperature variability in alpine terrain. *Cryosphere*. 2011;5(2):431-443. doi:10.5194/tc-5-431-2011
61. Gruber S, Hoelzle M, Haeberli W. Permafrost thaw and destabilization of Alpine rock walls in the hot summer of 2003. *Geophys Res Lett*. 2004;31(13):n/a. doi:10.1029/2004GL020051
62. Mittaz C, Hoelzle M, Haeberli W. First results and interpretation of energy-flux measurements over Alpine permafrost. *Ann Glaciol*. 2000;31:275-280. doi:10.3189/172756400781820363

SUPPORTING INFORMATION

Additional supporting information can be found online in the Supporting Information section at the end of this article.

How to cite this article: Magnin F, Ravanel L, Bodin X, et al. Main results of permafrost monitoring in the French Alps through the *PermaFrance* network over the period 2010–2022. *Permafrost and Periglac Process*. 2023;1-21. doi:10.1002/ppp.2209